Titolo

Sviluppo di un modello di dinamica di nocciolo per un DEMO LFR

Ente emittente   CIRTEN

PAGINA DI GUARDIA

Descrittori

Tipologia del documento:	Rapporto Tecnico
Collocazione contrattuale:	Accordo di programma ENEA-MSE: tema di ricerca "Nuovo nucleare da fissione"
Argomenti trattati:	Reattori nucleari veloci
	Generation IV reactors
	Reattori e sistemi innovativi

Sommario

E' stato sviluppato, per il reattore dimostrativo raffreddato a piombo, un modello semplificato di dinamica di nocciolo che permette un approccio preliminare alle problematiche di controllo del sistema. Questo consente un'analisi relativamente veloce della dinamica e della stabilità del sistema, che non può essere tralasciata in fase di progettazione. Il modello adottato, basato sull'approssimazione point-kinetics e su un modello di scambio di calore a temperature medie, è comunque in grado di considerare i principali feedback che controreazionano la variazione di reattività a fronte dei principali transitori operativi ed incidentali, tenendo conto sia della neutronica, della termo-idraulica e della espansione termo-meccanica.
Sono state quindi analizzate le risposte del reattore (in termini di escursione di temperatura del combustibile MOX e della guaina in acciaio ferritico-martensitico T91) ad eventi iniziatori di transitori, sia ad inizio sia a fine ciclo, implementando il modello sviluppato sulla piattaforma MATLAB/SIMULINK®.

Note

REPORT LP3.G2 – PAR 2007

Autori: Sara Bortot*, Antonio Cammi*, Patrizio Console Camprini**, Carlo Artioli***
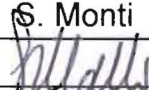
*Politecnico di Milano, Dipartimento di Energia, Sezione Ingegneria Nucleare-CeSNEF
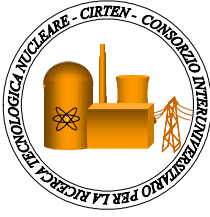
**Università di Bologna, Dipartimento di Ingegneria Energetica, Nucleare e del Controllo Ambientale (DIENCA)

***ENEA

Copia n.   **In carico a:**

2			NOME				
			FIRMA				
1			NOME				
			FIRMA				
0	**EMISSIONE**	23.9.2010	NOME	NA	S. Monti		NA
			FIRMA				
REV.	**DESCRIZIONE**	**DATA**		**CONVALIDA**	**VISTO**		**APPROVAZIONE**

CIRTEN

Consorzio Interuniversitario

per la Ricerca Tecnologica Nucleare

POLITECNICO DI MILANO

DIPARTIMENTO DI ENERGIA, Sezione INGEGNERIA NUCLEARE-CeSNEF*

UNIVERSITA' DI BOLOGNA

DIPARTIMENTO DI INGEGNERIA ENERGETICA, NUCLEARE e del CONTROLLO AMBIENTALE (DIENCA)**

ENEA

Centro Ricerche Bologna***

Sviluppo di un modello di dinamica di nocciolo per un DEMO LFR

Sara Bortot*, Antonio Cammi*, Patrizio Console Camprini, Carlo Artioli*****

CIRTEN-POLIMI RL 1138/2010

Milano, Agosto 2010

INDEX

EXECUTIVE SUMMARY

This document presents the status of development of a core dynamics model for a Generation IV Lead-cooled Fast Reactor (LFR) demonstrator (DEMO). A preliminary approach to the simulation of a core dynamics has been developed to provide a helpful tool in this early phase of the reactor pre-design -in which all the system specifications are still considered to be open design parameters-, allowing a relatively quick, qualitative analysis of dynamics and stability aspects that cannot be left aside when refining or even finalizing the system configuration.

Reactivity coefficients and kinetics parameters have been estimated for both Beginning of Cycle (BoC) and End of Cycle (EoC) core configurations (see also G. Grasso et al., "Progettazione concettuale di un nocciolo di impianto dimostrativo di LFR", linea progettuale LP3 – punto G1). A simplified lumped-parameter model reckoning with all the main feedbacks following a reactivity change in the core has been then developed to treat both neutronics and thermal-hydraulics: indeed, the point-kinetics approximation has been employed and an average-temperature heat-exchange model has been implemented. The latter sub-systems have been coupled and DEMO core responses to operational transient initiators -such as coolant inlet temperature perturbation or control rod withdrawal- at BoC and EoC have been finally analyzed using the MATLAB/SIMULINK® tool.

Space-time and point kinetics models have been then employed to provide preliminary indications of the core local behaviour following a transient, so as to primarily assess the excursions that MOX fuel and T91 ferritic-martensitic steel (FMS) cladding temperatures undergo, as they are subject to the most restricting technological constraints, whose respect must be guaranteed.

A further study has been begun aimed at addressing also the dynamic mechanical behaviour of DEMO core, by considering expansions and contractions instantaneous with temperature variations, i.e. neglecting mass inertia effects.

1   INTRODUCTION

The Lead-cooled Fast Reactor (LFR), being one of the six innovative systems selected by the Generation IV International Forum (GIF), is under development worldwide as a very promising fast neutron system to be operated in a closed fuel cycle [1]. In particular, within the 6th and 7th EURATOM Framework Programmes the European LFR community is proposing the ELSY - European Lead-cooled SYstem concept [2], an innovative 600 MW$_e$ pool-type LFR fully complying with Generation IV goal of sustainability and, in particular, aiming at no net production of Minor Actinides (MAs).

As recognized by the Strategic Research Agenda worked out by the European Sustainable Nuclear Energy Technology Platform (SNETP), LFR complete development requires -as a fundamental intermediate step- the realization of a demonstration plant (DEMO), intended to validate LFR technology as well as the overall system behaviour [3]. Indeed, a demonstration reactor is expected to prove the viability of technology to be implemented in the First-of-a-Kind industrial power plant.

In order to define a first reference configuration of a GENIV LFR DEMO, an I-NERI (International Nuclear Energy Research Initiative) agreement between the National Agency for the New Technologies, Energy and Environment (ENEA) and Argonne National Laboratory (ANL) has been signed in 2007. From the Italian side the work is being carried out in the frame of the national R&D program on "New Nuclear Fission" supported by the Italian Minister of Economic Development (MED) through a general Agreement with ENEA and the Italian University Consortium (CIRTEN).

In such a context, a reference configuration for a 300 MW$_{th}$ pool-type LFR DEMO is being developed and a static neutronics and thermal-hydraulics characterization has been accomplished [4].

Due to the need of investigating reactor responses to temperature transients, a preliminary approach concerning the simulation of DEMO core dynamics has been developed, in order to provide a helpful tool in this early phase of the reactor pre-design -in which all the system specifications are still considered to be open design parameters-, allowing a relatively quick, qualitative analysis of fundamental dynamics and stability aspects that cannot be left aside when refining or even finalizing the system configuration.

In this perspective, reactor dynamics is of primary importance for the study of plant global performances and for the design of an appropriate control system, since it explains the interactions among input and output variables and the nature of the basic dynamic relationships.

Many effects must be taken into account simultaneously for an accurate simulation: the coupling of different physical subsystems (i.e., neutronics, thermal-hydraulics, etc.) is concerned with the complexity of the large number of phenomena involved, and with the approximations necessarily employed to implement the model (geometrical arrangement description as well as mathematical and numerical treatment).

A simplified lumped-parameter model reckoning with all the main feedbacks following a reactivity change in the core has been then developed to treat both neutronics and thermal-hydraulics. Indeed, it has been assumed that neutron time fluctuations and spectrum are independent of spatial variations and neutron level, respectively. Accordingly, the core has been considered as a lumped source of neutrons with prompt heat power, with neutron population and neutron flux related by constants of proportionality, leading to the point-kinetics approximation to be employed [5].

A zero-dimensional approach has been adopted to treat also the system thermal-hydraulics. Some simplifying hypotheses have been assumed and a single-node heat-exchange model has been implemented by accounting of three

distinct temperature regions –corresponding to fuel, cladding and coolant-, enabling reactivity feedback to include all the major contributions. In line with the point model concept, fuel, cladding and coolant temperatures have been assumed to be functions separable in space and time.

Neutron kinetics has been then coupled with heat transfer dynamics through reactivity feedback coefficients -generated by change in neutron cross sections due to fuel Doppler and coolant density effects and by core thermal expansions-, which have been estimated for both Beginning of Cycle (BoC) and End of Cycle (EoC) core configurations by means of ERANOS (European Reactor ANalysis Optimised System) deterministic code ver. 2.1 [6] coupled with JEFF-3.1 data library [7], as well as the corresponding kinetics parameters.

DEMO dynamic behaviour has been studied through a simplified linearized model -based on a small perturbation approach-, which has been handled in terms of state, input and output variables, according to the theory of linear systems. The Laplace-transformed equations have been solved simultaneously by means of a matrix equation so as to evaluate the system representative transfer functions. Core responses to operational transients initiators -such as coolant inlet temperature stepwise perturbation or control rod withdrawal- at BoC and EoC have been finally analyzed using the MATLAB/SIMULINK[®] tool [8, 9], in order to assess the excursions that MOX fuel and T91 ferritic-martensitic steel (FMS) cladding temperatures undergo, since they are subject to the most restricting technological constraints whose respect must be guaranteed during any operational transient [4]. The analysis of DEMO core sub-system open-loop stability has ultimately been performed.

A preliminary study of DEMO core kinetics has been then associated to dynamic investigations: the ERANOS KIN3D module [10] has been employed to accomplish simulations of reactor transients induced by both fuel temperature and coolant temperature variations, and a control rod complete withdrawal and insertion.

Material density and temperature distributions obtained from the previous coupled point-kinetics and thermal-hydraulics model have been employed to compute effective neutron cross-sections for reactor sub-regions that have been used as input data for core neutronics calculations.

Finally, an alternative dynamic model of DEMO has been implemented in order to approach the problem of the core mechanical behaviour, which has been initially coped with by neglecting mass inertia effects.

2 DEMO DYNAMICS STUDY

2.1 DEMO core configuration

In the current design, DEMO features a 300 MW_{th} MOX-fuelled core, composed by wrapper-less square fuel assemblies (FAs) with pins arranged in a square lattice; 10 FAs with 29.3 vol.% Pu fraction constitute the inner zone, and 14 FAs with 32.2 vol.% Pu fraction compose the outer zone.

As far as FA design, fuel pins are arranged in a 28×28 square lattice, every FA being provided with 4 structural uprights at corners connected with the central FMS T91 box beam replacing 6×6 central positions.

Two different and independent control rod systems guarantee the required reliability for reactor shut-down and safety: 4 passive B_4C (90 at.% enrichment in [10]B) Finger Absorber Rods (FARs) carry out exclusively SCRAM purposes, being positioned outside the active core in normal operation; 20 motorized B_4C (42 at.% enrichment in [10]B) FARs are demanded for cycle reactivity swing control and safe shut-down, 16 of which being inserted for half active height (BoC reference configuration) or positioned 1 cm above the active core (EoC reference configuration) respectively.

Fig. 1 shows (on the left) a radial section of the core composed by 24 FAs surrounded by dummy assemblies, and (on the right) a bi-dimensional RZ representation of the vertical section that yields a useful scheme for the main structural zones.
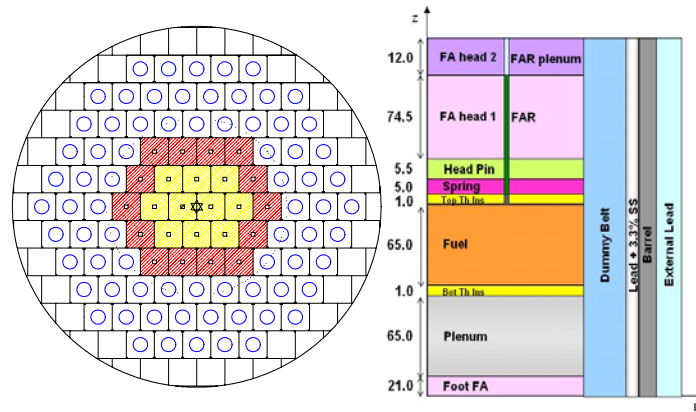

Fig. 1. Core layout (left) and 2D RZ cylindrical section (right); dimensions in cm.

In Table I the main DEMO core specifications are summarized.

TABLE I

DEMO major core specifications, cold dimensions (20 °C).

Parameter	Value	Unit
Thermal Power	300	MW_{th}
Average Coolant Outlet Temperature	480	°C
Coolant Inlet Temperature	400	°C
Average Coolant Velocity	3.0	$m\ s^{-1}$
Cladding Maximum Temperature	600	°C
Cladding Outer Diameter	6.00	mm
Cladding Thickness	0.34	mm
Pellet Outer Diameter	5.14	mm
Pellet Hole Diameter	1.71	mm
Fuel Column Height	650	mm
Fuel Rod Pitch	8.53	mm
Number of Pins/FA	744	-
FMS box beam inner width	45.65	mm
FMS box beam outer width	48.65	mm
Number of Inner/Outer FAs	10/14	-
Pu Fraction Inner/Outer Zone	29.3/32.2	vol.%

2.2 Reactivity coefficients

Neutronics analyses have been performed by means of ERANOS deterministic code ver. 2.1 in conjunction with JEFF-3.1 data library.

Multi-group cross-sections associated to every reactor zone shown in Fig. 1 have been retrieved from ECCO (European Cell COde) [11] calculations. A very refined cell description has been adopted for both FAs and subcritical zones surrounding the active core (with the exception of dummy radial reflector assemblies): they have been described by an accurate heterogeneous geometry model, whereas the remaining ones (namely 'Foot FA', 'Dummy Belt', 'Barrel' and 'External Lead') have been described by a homogeneous cell geometry model. In both cases, ECCO computations have been carried out by treating the main nuclides with a fine energy structure (1968 groups) and condensing the obtained cross-sections into 33 groups.

The reference working temperatures which have been assumed are the following: in the active core zone, 900 °C for the fuel, 440 °C for structures and coolant, 480 °C for the cladding; for subcritical cells, 400 °C for zones below the active zone, 480 °C above the active zone, and 440 °C for lateral zones.

ECCO evaluations have finally been used to set tri-dimensional core models up; then the whole system has been solved through nodal transport calculations by means of the ERANOS TGV/VARIANT module [12].

In the reference configurations the reactor is characterized by a multiplication factor k_{eff} = 1.00033 (ρ = 33 pcm) and k_{eff} = 1.00093 (ρ = 93 pcm) at BoC and EoC, respectively.

In order to estimate the Doppler and the coolant density feedback effects, the following deviations from the nominal parameters have been applied:

- fuel temperature raise (variation: + 326.85 K);
- coolant density reduction in the active core zone (variation: - 5%).

Furthermore, elementary perturbations have been introduced in order to figure radial and axial expansion reactivity coefficients through a "partial derivative" approach. Such a method is based on the main hypothesis of superposition principle validity and of linear response of the system within the interval defined by the reference and the perturbed configurations as well.

The following elementary perturbations have been applied:

- core radial extension by scaling all radial dimensions, with nominal densities (variation: + 2.5%);
- core axial extension by scaling all axial dimensions, with nominal densities (variation: + 5%);
- fuel density reduction (variation: - 5%);
- steel density reduction (variation: - 5%);
- absorber density reduction (variation: - 10%).

The latter have been then composed to compute the main reactivity coefficients as described in the following sections.

Doppler Coefficient

The Doppler effect can be evaluated according to the relation:

$$d\rho = \alpha \frac{dT}{T} \tag{1}$$

With respect to the considered temperature variation (from 1173.15 to 1500 K), the Doppler coefficient results $\alpha_D = -0.177/-0.202$ pcm K^{-1} at BoC and EoC, respectively.

Since the reactivity change is strongly dependent (logarithmic behaviour) on the temperature variation involved, the Doppler constant α is provided owing to its more general applicability: $\alpha = -235/-268$ pcm. Its rather low value is justified by the high Pu fraction, which weakens the effect of ^{238}U macroscopic absorptions in epithermal region.

Coolant Density Coefficient

The coolant density reactivity coefficient can be computed by referring to the following expression:

$$\left. \frac{d\rho}{dT} \right|_{coolant} = \frac{\partial P}{\partial\left(\dfrac{\delta P_{cool}}{P_{cool}} \right)} \frac{d\left(\dfrac{\delta P_{cool}}{P_{cool}} \right)}{dT} \tag{2}$$

Considering the elementary perturbations and the coolant thermal expansion [13], the coolant density coefficient results $\alpha_L = -0.120/-0.141$ pcm K^{-1} at BoC and EoC, respectively.

Radial Expansion Coefficient

Despite the fact that no diagrid is foreseen in DEMO design, the traditional reactivity effect due to its radial expansion can be calculated thanks to the continuous lattice formed by FA foots [14] according to:

$$\left. \frac{d\rho}{dT} \right|_{diagrid} \approx l_{T91}(T_{in}) \left\{ \frac{\partial\rho}{\partial\left(\dfrac{\delta R}{R} \right)} - 2\left[\frac{\partial\rho}{\partial\left(\dfrac{\delta P_{fuel}}{P_{fuel}} \right)} + \frac{\partial\rho}{\partial\left(\dfrac{\delta P_{absorber}}{P_{absorber}} \right)} + \frac{\partial\rho}{\partial\left(\dfrac{\delta P_{steel}}{P_{steel}} \right)} + \left(1 - \frac{1}{f_{coolant}}\right)\frac{\partial\rho}{\partial\left(\dfrac{\delta P_{coolant}}{P_{coolant}} \right)} \right] \right\} \tag{3}$$

where the T91 linear expansion coefficient has been evaluated at the nominal lead inlet temperature [15].

The reactivity coefficient due to the diagrid-equivalent radial expansion results $\alpha_R = -0.871/-0.923$ pcm K^{-1} at BoC and EoC, respectively.

An alternative value for the core radial expansion coefficient has been calculated considering the radial expansion to be driven by the coolant inlet temperature T_l, leading to $\alpha_R = -0.886/-0.939$ pcm K^{-1} at BoC and EoC, respectively.

Axial Expansion Coefficient

The elementary reactivity variations have been properly combined in order to obtain the equivalent coefficient due to the core axial expansion according to:

$$\frac{d\rho}{dT}\bigg|_{axial} \approx \frac{1}{T_{mat*,out} - T_{mat*,in}} \int_{T_{mat*,in}}^{T_{mat*,out}} l_{mat}(T)dT \left[\frac{\partial \rho}{\partial\left(\frac{\delta Z}{Z}\right)} - \left(\frac{\partial \rho}{\partial\left(\frac{\delta P_{fuel}}{P_{fuel}}\right)} + \frac{\partial \rho}{\partial\left(\frac{\delta P_{steel}}{P_{steell}}\right)} \right) \right] + \frac{\partial \rho}{\partial L_{insertion}} \frac{dL_{insertion}}{dT} \tag{4}$$

The contribution of the dislocation of FARs due to their differential expansion with respect to the active core has been accounted of by considering the dilations of both the hot leg and the active core instantaneous [14], as follows:

$$dL_{insertion} = dL_{hot-leg} + dL_{core} \tag{5}$$

where the first term has been calculated as:

$$dL_{hot-leg} = L_{hot-leg}(T_{out})l_{T91}(T_{out})dT \tag{6}$$

and the dilation of the core portion interested by the insertion of FARs (assumed L_{FARs}) has been written as:

$$dL_{core} = \left(\int_{L_{FARs}}^{Z_{fuel}} l_{T91}(L)dL \right)dT \tag{7}$$

in the linked case, and

$$dL_{core} = \left(\int_{0}^{Z_{fuel}} l_{T91}(L)dL \right)dT - \left(\int_{0}^{L_{FARs}} l_{MOX}(L)dL \right)dT \tag{8}$$

in the not-linked case, where the concerned linear expansion coefficients have been properly evaluated on the basis of both the steel- and fuel-related values in correspondence to the respective theoretical mean temperatures at steady-state [15, 16].

Coherently, the axial expansion coefficient turns out to be $\alpha_Z = 0.009/- 0.195$ pcm K^{-1} (BoC/EoC) in the linked case, and $\alpha Z = 0.033/- 0.191$ pcm K^{-1} (BoC/EoC) in the not-linked case.

2.3 Mathematical model

The model developed is based upon the fundamental conservation equations and employs a lumped parameters approach for the coupled kinetics (six delayed neutron precursor groups point reactor) and thermal-hydraulics, with continuous reactivity feedback due to temperature effects. A simplified block-scheme of DEMO primary system -assumed to consist only of the active core, disregarding both upper and lower plena- has been adopted: the thermal-hydraulics sub-system has been described by zero-dimensional, single phase, single channel conservation

equations. Fuel, cladding and coolant temperatures have been determined through an energy balance over the average pin surrounded by coolant, in which reactor power is an input variable retrieved from reactor kinetics (coherently with the approximation of accounting only for the total power generated by fission, neglecting the contribution of decay heat). The so-calculated thermal-hydraulic parameters have been finally employed to insert the reactivity feedbacks into the neutronics equations, as shown in Figure 2.
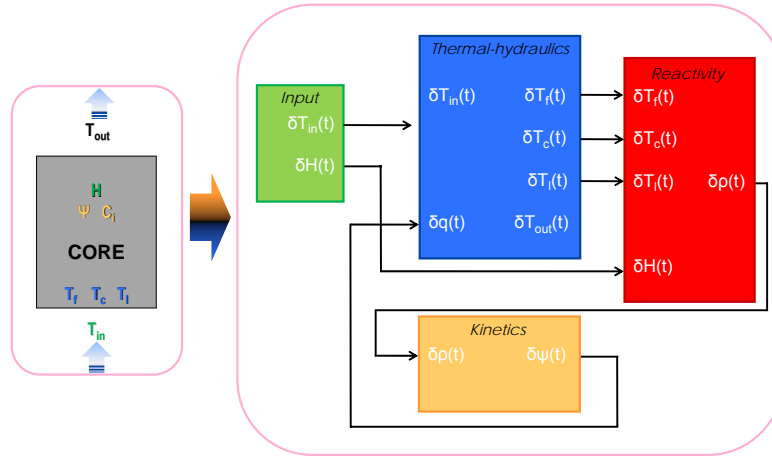
Fig. 2. DEMO core block scheme.

Neutron Kinetics Equations

The one prompt group point kinetics formulation of the neutron density can be written as [5]:

$$\frac{dn(t)}{dt} = \frac{\rho - \beta}{\Lambda} n(t) + \sum_{1}^{6} \lambda_i C_i(t) \tag{9}$$

the corresponding concentration of the six precursor groups of delayed neutrons being expressed as:

$$\frac{dC_i(t)}{dt} = \frac{\beta_i}{\Lambda} n(t) - \lambda_i C_i(t) \cdot \tag{10}$$

As a further assumption, the system has been considered at steady-state for $t \leq 0$.

A small perturbation approach has been applied, given that the point kinetics model is computationally efficient and can provide accurate results for small reactor perturbations when "true" time-dependent distributions of power and reactivity coefficients close to their steady-state distributions may be assumed.

Consequently, Eq. (9) and (10) have been perturbed around their steady-state solutions and then linearized obtaining seven linear equations describing the neutron kinetics behaviour in terms of dimensionless variables:

$$\frac{d\delta\psi(t)}{dt} = -\frac{\beta}{\Lambda} \delta\psi(t) + \frac{1}{\Lambda} \sum_{1}^{6} \beta_i \delta\eta_i(t) + \frac{\delta\rho(t)}{\Lambda} \tag{11}$$

$$\frac{d\,\delta\eta_i(t)}{dt} = \lambda_i \delta\psi(t) - \lambda_i \delta\eta_i(t) \, , \tag{12}$$

being $\psi = n(t)/n_0 = q(t)/q_0$ and $_{\eta i} = C_i(t)/Ci0$.

Reactivity and Feedback Function

Consistently with the lumped parameter modelling employed, reactivity feedback has been expressed as a function of the mean values of fuel, cladding and coolant temperatures, and core inlet temperature. Moreover, externally introduced reactivity has been simulated by the coefficient α_H associated with the insertion length of an ideal control rod, which has handled as a simple input parameter.

Under the hypotheses of small perturbations, reactivity depends linearly on constant coefficients associated with the respective parameter variation from its steady-state value; therefore, continuous reactor feedbacks have been calculated as follows (reference calculations):

$$\delta\rho(t) = \alpha_D \delta T_f + \alpha_Z \delta T_c + \alpha_l \delta T_l + \alpha_R \delta T_{in} + \alpha_H \delta H \tag{13}$$

In the above expression the first and the third terms in the right-hand side represent respectively the feedbacks induced by fuel (Doppler effect) and coolant (coolant density effect) temperature changes.

Coherently with the assumption of closed gap between fuel and cladding at both BoC and EoC, the axial expansion has been expressed as a function of cladding temperature variation (second term). Withal, the radial expansion coefficient has been associated with the coolant inlet temperature, since it governs the expansion of the continuous lattice formed by FA foots.

The impact of assuming the pellet column to be not-linked to the cladding –and consequently the axial expansion to be controlled by the fuel temperature-, and the radial expansion to be driven by the coolant average temperature has been further assessed, the corresponding reactivity equations having been expressed as follows:

$$\delta\rho(t) = (\alpha_D + \alpha_Z)\delta T_f + \alpha_l \delta T_l + \alpha_R \delta T_{in} + \alpha_H \delta H \tag{14}$$

and

$$\delta\rho(t) = \alpha_D \delta T_f + \alpha_Z \delta T_c + (\alpha_l + \alpha_R)\delta T_l + \alpha_H \delta H \tag{15}$$

Thermal-hydraulics Equations

The equations below describe the single node transient behaviour of fuel, cladding and coolant temperatures in the active core region.

For the gradient of the average fuel temperature, the heat transfer process has been achieved by taking an energy balance over an ideal fuel element:

$$M_f C_f \frac{dT_f(t)}{dt} = q(t) - k_{fc}(T_f(t) - T_c(t)), \tag{16}$$

where:

- properties and thermal resistances of fuel, gap and cladding have been assumed constant with temperature and time;

- the global heat transfer coefficient k_{fc}, describing a combined heat transfer coefficient from fuel to cladding surface, has been determined by using a separate, multi-zone fuel pin model which accounts of the temperature distribution from the fuel centreline to the cladding surface [4], has been calculated in correspondence to the average nominal temperatures and kept constant throughout the dynamic analysis;

- conduction in the axial direction has been neglected;

- the power generated in the fuel by fission has been obtained from neutron kinetics equations (according to the relation $n(t)/n_0 = q(t)/q_0$) and has been treated as an input for the heat transfer dynamic model.

For the gradient of the cladding surface temperature, the following energy balance has been applied:

$$M_c C_c \frac{dT_c(t)}{dt} = k_{fc}(T_f(t) - T_c(t)) - h_{cl}(T_c(t) - T_l(t)), \tag{17}$$

Finally, the energy balance equation for the coolant, by using the symmetrical definition of $T_l = (T_{in} + T_{out})/2$ in which the lead inlet temperature is an input variable, has been written as:

$$M_l C_l \frac{dT_l(t)}{dt} = h_{cl}(T_c(t) - T_l(t)) - \Gamma C_l(2T_l(t) - 2T_{in}(t)), \tag{18}$$

where the heat transfer coefficient has been determined from Zhukov correlation [16].

Eq. (16), (17) and (18) have been perturbed around the steady-state and linearized in turn, leading to:

$$\frac{d\delta T_f(t)}{dt} = -\frac{1}{\tau_f}\delta T_f(t) + \frac{1}{\tau_f}\delta T_c(t) + \frac{q_0}{M_f C_f}\delta\psi(t) \tag{19}$$

$$\frac{d\delta T_c(t)}{dt} = \frac{1}{\tau_{c1}}\delta T_f(t) + \left(-\frac{1}{\tau_{c1}} - \frac{1}{\tau_{c2}}\right)\delta T_c(t) + \frac{1}{\tau_{c2}}\delta T_l(t) \tag{20}$$

$$\frac{d\delta T_l(t)}{dt} = \frac{1}{\tau_l}\delta T_c(t) + \left(-\frac{1}{\tau_l} - \frac{2}{\tau_0}\right)\delta T_l(t) + \frac{2}{\tau_0}\delta T_{in}(t), \tag{21}$$

with time constants $\tau_f = (M_f C_f)/k_{fc}$, $\tau_{c1} = (M_c C_c)/k_{fc}$, $\tau_{c2} = (M_c C_c)/h_{cl}$, $\tau_l = (M_l C_l)/h_{cl}$ and $\tau_0 = M_l/\Gamma$.

2.4 Simulations and results

The modelling equations described above have been handled in terms of state vector ($\underline{X}$), input vector ($\underline{U}$), output vector ($\underline{Y}$), corresponding matrices ($\underline{\underline{A}}$, $\underline{\underline{B}}$ and $\underline{\underline{C}}$ respectively) and feed-through matrix $\underline{\underline{D}}$, leading to the following state space representation [18]:

$$\begin{cases} \underline{\dot{X}} = \underline{\underline{A}}\,\underline{X} + \underline{\underline{B}}\,\underline{U} \\ \underline{Y} = \underline{\underline{C}}\,\underline{X} + \underline{\underline{D}}\,\underline{U} \end{cases} \tag{22}$$

where, in the BoC and EoC reference models,

$$\underline{\underline{A}} = \begin{bmatrix} \frac{1}{\tau_f} & \frac{1}{\tau_f} & 0 & \frac{q_0}{M_f C_f} & 0 & 0 & 0 & 0 & 0 & 0 \\ \frac{1}{\tau_{c1}} & \left(\frac{1}{\tau_{c1}} - \frac{1}{\tau_{c2}}\right) & \frac{1}{\tau_{c2}} & 0 & 0 & 0 & 0 & 0 & 0 & 0 \\ 0 & \frac{1}{\tau_l} & \left(\frac{1}{\tau_l} - \frac{2}{\tau_0}\right) & 0 & 0 & 0 & 0 & 0 & 0 & 0 \\ \frac{\alpha_D}{\Lambda} & \frac{\alpha_Z}{\Lambda} & \frac{\alpha_L}{\Lambda} & \frac{\beta}{\Lambda} & \frac{\beta_1}{\Lambda} & \frac{\beta_2}{\Lambda} & \frac{\beta_3}{\Lambda} & \frac{\beta_4}{\Lambda} & \frac{\beta_5}{\Lambda} & \frac{\beta_6}{\Lambda} \\ 0 & 0 & 0 & \lambda_1 & -\lambda_1 & 0 & 0 & 0 & 0 & 0 \\ 0 & 0 & 0 & \lambda_2 & 0 & -\lambda_2 & 0 & 0 & 0 & 0 \\ 0 & 0 & 0 & \lambda_3 & 0 & 0 & -\lambda_3 & 0 & 0 & 0 \\ 0 & 0 & 0 & \lambda_4 & 0 & 0 & 0 & -\lambda_4 & 0 & 0 \\ 0 & 0 & 0 & \lambda_5 & 0 & 0 & 0 & 0 & -\lambda_5 & 0 \\ 0 & 0 & 0 & \lambda_6 & 0 & 0 & 0 & 0 & 0 & -\lambda_6 \end{bmatrix}$$

$$\underline{\underline{B}} = \begin{bmatrix} 0 & 0 \\ 0 & 0 \\ \frac{2}{\tau_0} & 0 \\ \frac{\alpha_R}{\Lambda} & \frac{\alpha_H}{\Lambda} \\ 0 & 0 \\ 0 & 0 \\ 0 & 0 \\ 0 & 0 \\ 0 & 0 \\ 0 & 0 \end{bmatrix} \quad \underline{\underline{C}} = \begin{bmatrix} 1 & 0 & 0 & 0 & 0 & 0 & 0 & 0 & 0 & 0 \\ 0 & 1 & 0 & 0 & 0 & 0 & 0 & 0 & 0 & 0 \\ 0 & 0 & 1 & 0 & 0 & 0 & 0 & 0 & 0 & 0 \\ 0 & 0 & 2 & 0 & 0 & 0 & 0 & 0 & 0 & 0 \\ 0 & 0 & 0 & 1 & 0 & 0 & 0 & 0 & 0 & 0 \\ 0 & 0 & 0 & q_0 & 0 & 0 & 0 & 0 & 0 & 0 \\ \alpha_D & \alpha_Z & \alpha_L & 0 & 0 & 0 & 0 & 0 & 0 & 0 \end{bmatrix} \quad \underline{\underline{D}} = \begin{bmatrix} 0 & 0 \\ 0 & 0 \\ 0 & 0 \\ -1 & 0 \\ 0 & 0 \\ 0 & 0 \\ \alpha_R & \alpha_H \end{bmatrix}$$

The MIMO (Multi Input – Multi Output) system described by Eq. (22) has been directly simulated in MATLAB [8], once the four matrices have been obtained. It presents ten state variables: (namely, variations of: fuel, cladding and coolant average temperatures, neutron population, and neutron precursors), two inputs (namely, variations of lead inlet temperature and control rod extraction length) and seven outputs (namely, variations of: fuel, cladding and coolant average temperatures, core outlet temperature, neutron population, core power and reactivity):

$$\underline{X} = \begin{bmatrix} \delta T_f \\ \delta T_c \\ \delta T_l \\ \delta \psi \\ \delta \eta_1 \\ \delta \eta_2 \\ \delta \eta_3 \\ \delta \eta_4 \\ \delta \eta_5 \\ \delta \eta_6 \end{bmatrix} \qquad \underline{Y} = \begin{bmatrix} \delta T_f \\ \delta T_c \\ \delta T_l \\ \delta T_{out} \\ \delta \psi \\ \delta q \\ \delta \rho \end{bmatrix} \qquad \underline{U} = \begin{bmatrix} \delta T_{in} \\ \delta H \end{bmatrix}$$

In Tables II and III the main input data pertaining severally to the reference BoC and EoC configurations are given (ERANOS-2.1, JEFF-3.1 data library calculations). Input parameters have been perturbed in order to investigate the

open loop dynamic behaviour of DEMO core, as well as to observe and compare BoC and EoC new equilibrium configurations after the transients. In particular, the effects of lead inlet temperature increase ($+ 10\,K$ compared to its nominal value), and of an ideal control rod extraction (corresponding to a reactivity step of $+ 50\,pcm$) have been analyzed separately. Simulations have been started at initial time $1\,s$ and run for $300\,s$, in order for the asymptotic output values to be reached.

TABLE II

DEMO core BoC reference data.

Quantity	Value	Units	Quantity	Value	Units
β_1	6.142	pcm	α	- 235	pcm
β_2	71.40	pcm	α_D	- 0.1774	pcm K^{-1}
β_3	34.86	pcm	α_H	187	pcm cm^{-1}
β_4	114.1	pcm	α_L	- 0.1204	pcm K^{-1}
β_5	69.92	pcm	α_R	- 0.8715	pcm K^{-1}
β_6	22.68	pcm	α_Z	0.0088	pcm K^{-1}
λ_1	0.0125	s^{-1}	τ_f	1.94	s
λ_2	0.0292	s^{-1}	τ_{c1}	0.87	s
λ_3	0.0895	s^{-1}	τ_{c2}	0.06	s
λ_4	0.2575	s^{-1}	τ_l	0.16	s
λ_5	0.6037	s^{-1}	τ_0	0.21	s
λ_6	2.6688	s^{-1}	M_f	2391	kg
Λ	$8.0659 \cdot 10^{-7}$	s	C_f	317.5	J kg^{-1} K^{-1}
β	319	pcm	q_0	$300 \cdot 10^6$	W

TABLE III

DEMO core EoC reference data.

Quantity	Value	Units	Quantity	Value	Units
β_1	6.224	pcm	α	- 268	pcm
β_2	72.33	pcm	α_D	- 0.2019	pcm K^{-1}
β_3	35.34	pcm	α_H	70	pcm cm^{-1}
β_4	115.5	pcm	α_L	- 0.1408	pcm K^{-1}
β_5	70.75	pcm	α_R	- 0.9234	pcm K^{-1}
β_6	22.89	pcm	α_Z	- 0.1949	pcm K^{-1}
λ_1	0.0125	s^{-1}	τ_f	1.99	s
λ_2	0.0292	s^{-1}	τ_{c1}	0.89	s
λ_3	0.0895	s^{-1}	τ_{c2}	0.06	s
λ_4	0.2573	s^{-1}	τ_l	0.16	s
λ_5	0.6025	s^{-1}	τ_0	0.21	s
λ_6	2.6661	s^{-1}	M_f	2391	kg
Λ	$8.4980 \cdot 10^{-7}$	s	C_f	317.5	J kg^{-1} K^{-1}
β	323	pcm	q_0	$300 \cdot 10^6$	W

Lead Inlet Temperature Perturbation

The core inlet temperature has been enhanced by 10 K, leading to an insertion of negative reactivity (Fig. 3) due to both the instantaneous radial expansion and the lead density feedbacks, the latter being induced by the coolant average temperature increase (Fig. 4).
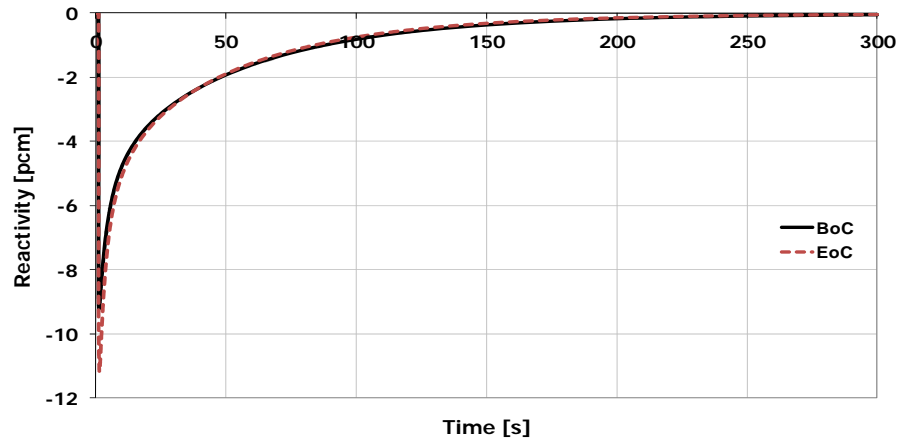

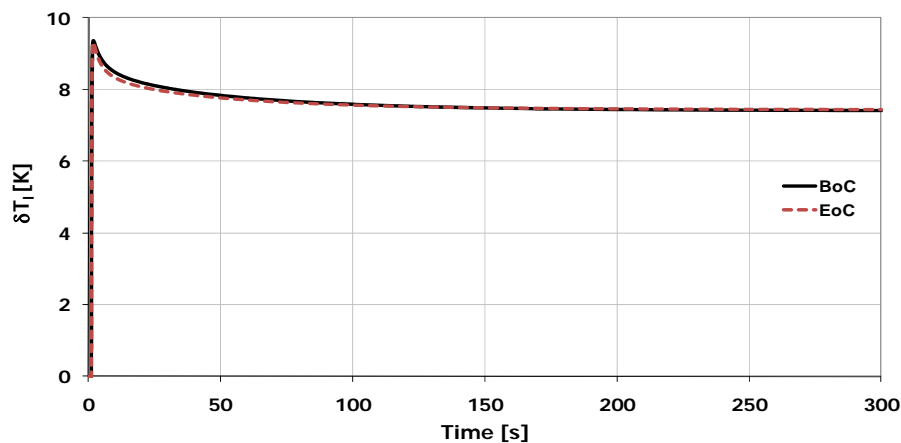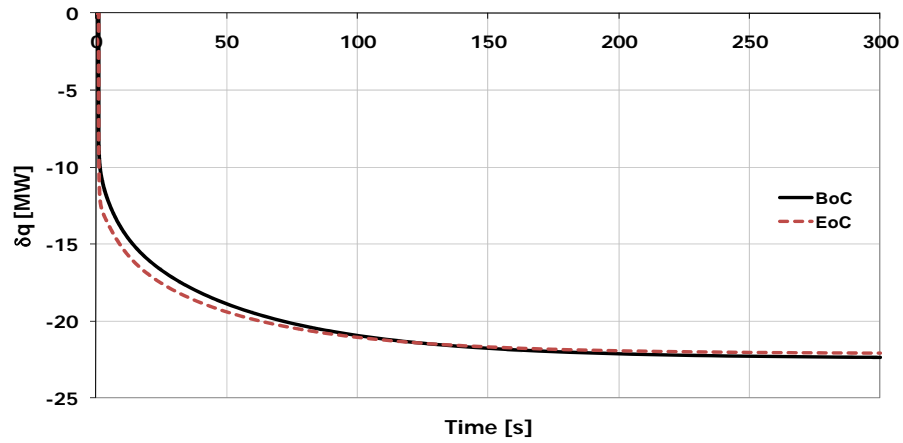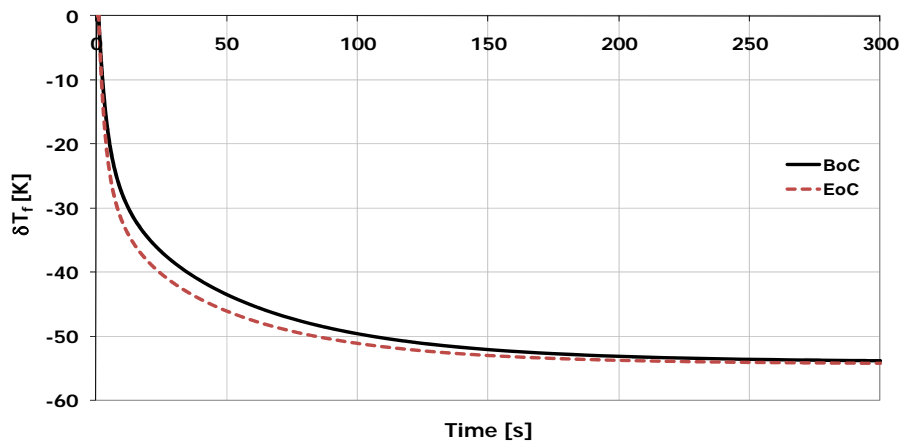Fig. 3. Core reactivity variation following an enhancement by 10 K of core inlet temperature.

Fig. 4. Lead average temperature variation following an enhancement by 10 K of core inlet temperature.

Because of the negative reactivity injection brought by higher lead temperatures, the core power undergoes a prompt decrease in the first part of the transient (Fig. 5), as far as the contribution of Doppler (due to the fuel average temperature reduction showed in Fig. 6) and axial expansion (due to the increased cladding temperature depicted in Fig. 7) start balancing the effects of lead temperature on reactivity at BoC.

The same general trend is observed also for the EoC situation, except for the opposite contribution of axial expansion to reactivity, which is negative. Indeed, only the Doppler effect is accountable for the reactivity raise after the peak of – 11 pcm (reached at time 0.5 s) caused by both higher coolant temperatures and core axial displacement.

Correspondingly, the reactivity increases again showing first a rapid rise and then a slower slope due to the opposing contribution of the axial contraction effect (at BoC), finally reinstating criticality.

Therefore, the reactor power stabilizes to a new equilibrium value, approximately 22.4 and 22.1 MW$_{th}$ lower than the nominal one at BoC and EoC, respectively.

Fig. 5. Reactor power variation following an enhancement by 10 K of core inlet temperature.

Fig. 6. Fuel average temperature variation following an enhancement by 10 K of core inlet temperature.
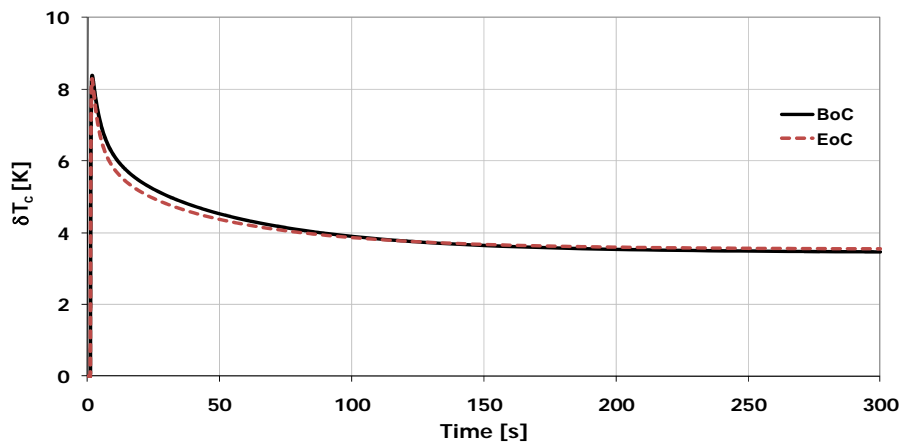
Fig. 7. Cladding average temperature variation following an enhancement by 10 K of core inlet temperature.

At the end of the transient, the lead outlet temperature shows a positive variation (+ 4.80/+ 4.88 K at BoC/EoC), as Fig. 8 illustrates, but smaller than both the inlet perturbation and the average coolant temperature enhancement (+ 7.40/+ 7.44 K at BoC/EoC), due to the decrease in reactor power outlined in Fig. 5. On the contrary, the fuel temperature response is monotonically negative and settles at - 53.9/- 54.3 K respectively.

As to cladding temperature, after the peak of + 8.36/+ 8.24 in the very first part of the transient, it eventually sets at a relative variation of + 3.44/+ 3.54 with respect to the steady state value.
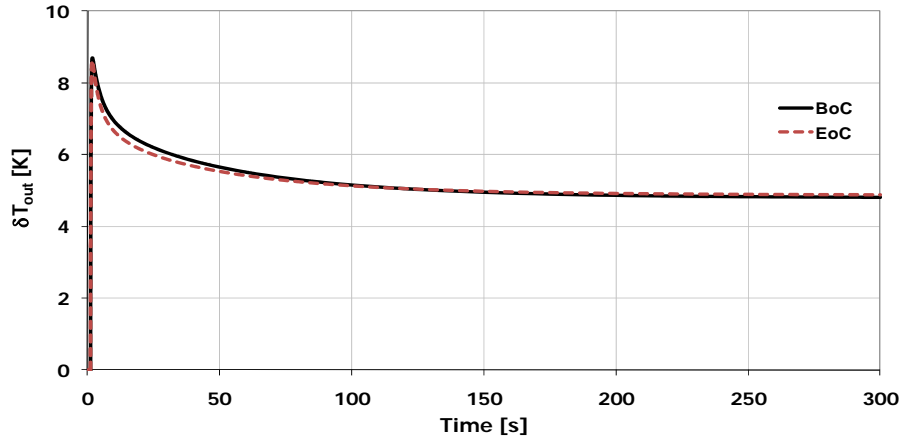
Fig. 8. Core outlet temperature variation following an enhancement by 10 K of core inlet temperature.

In order to verify the model prediction accuracy, the energy balance over the whole core has been calculated:

$$q = \Gamma C_l (T_{out} - T_{in}) = 2575 \cdot 71456 \cdot (48480 - 410) = 28051 \, MW \tag{23}$$

for the BoC situation, whereas for EoC:

$$q = \Gamma C_l (T_{out} - T_{in}) = 2575 \cdot 71456 \cdot (48488 - 410) = 28081 \, MW \tag{24}$$

Looking at the model results, the reactor thermal power (Fig. 5) after transient is found to be 277.6/277.9 MW$_{th}$, respectively, hence the error committed using a linearized model is almost negligible.

Control Rod Extraction

A further perturbation has been performed in order to evaluate DEMO dynamic response to a step reactivity insertion of 50 pcm (Fig. 9) at both BoC and EoC.

As Fig. 10 highlights, the expected response is observed, i.e. the initial, instantaneous power rise (prompt jump), whose time characteristic (0.6/0.5 s at BoC/EoC) and huge amplitude (50/48 MW$_{th}$ at BoC/EoC) are essentially determined by the prompt neutron life time and the delayed neutron fraction of the system.
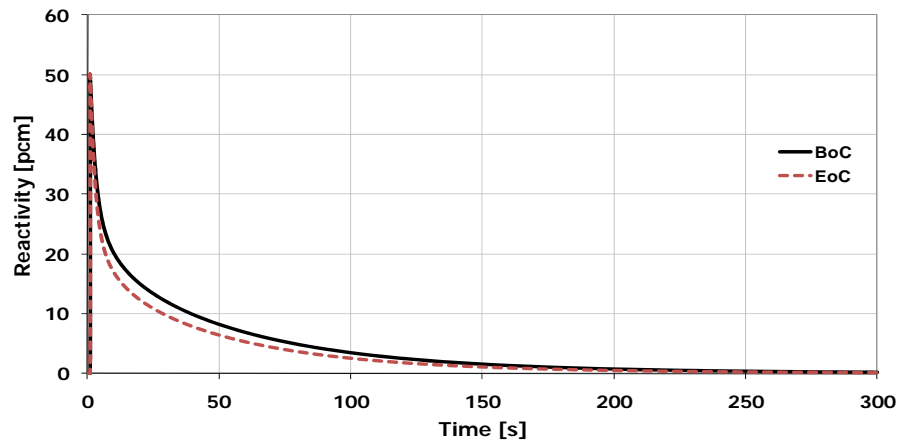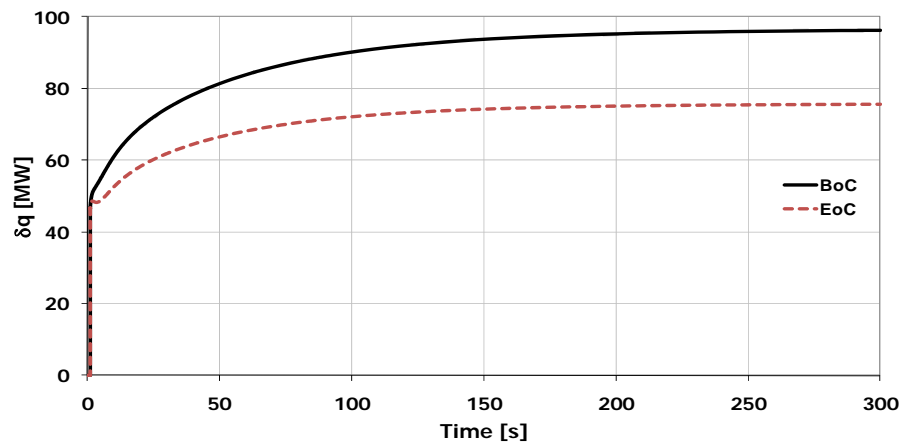
Fig. 9. Core reactivity variation following an externally given perturbation of 50 pcm.

As Fig. 10 highlights, the expected response is observed, i.e. the initial, instantaneous power rise (prompt jump), whose time characteristic (0.6/0.5 s at BoC/EoC) and huge amplitude (50/48 MW_{th} at BoC/EoC) are essentially determined by the prompt neutron life time and the delayed neutron fraction of the system.

Fig. 10. Reactor power variation following a step reactivity insertion of 50 pcm.

After the power high peak at the transient beginning, fuel and lead temperatures (Figs. 11 and 12) start rising monotonically so as to balance the positive reactivity introduced by extracting the ideal control rod.

At BoC the considerable increase of cladding temperature, which finally settles at a relative variation of + 28.3 K (Fig. 13), opposes the corresponding negative reactivity feedbacks; the reactor power rises to a new stable value, 96.6 MW_{th} higher than the nominal one. At EoC the negative feedback due to axial expansion combines to bring about the reactivity decrease; the reactor power finally sets at + 75.6 MW_{th}.
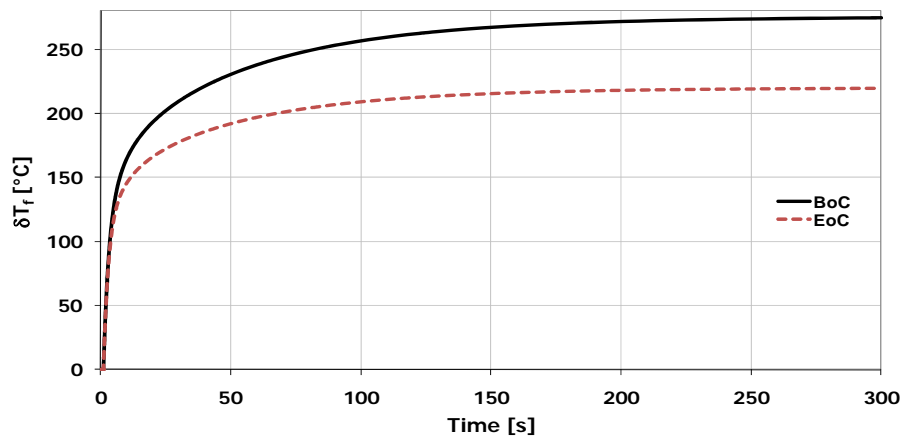
Fig. 11. Fuel average temperature variation following a step reactivity insertion of 50 pcm.
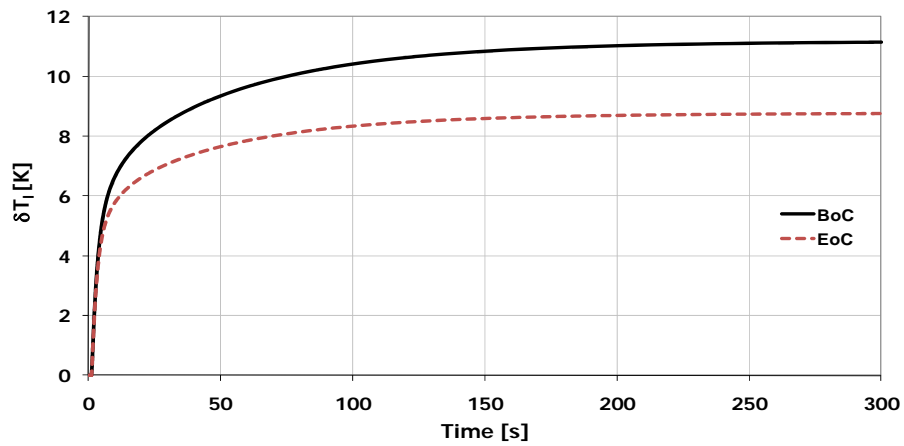
Fig. 12. Lead average temperature variation following a step reactivity insertion of 50 pcm.
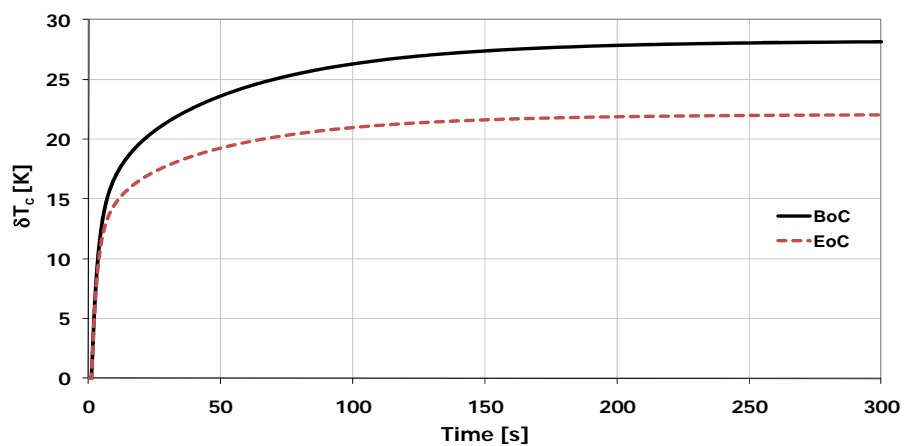
Fig. 13. Cladding average temperature variation following a step reactivity insertion of 50 pcm.

At the end of the transient, the fuel temperature variation results significantly positive in turn, tending asymptotically to + 276/+ 220 K at BoC/EoC.

As evident in Fig. 12, also the average coolant temperature features a positive variation of 11.2/8.8 K, and the lead outlet temperature shows an analogous trend but characterized by a major amplitude, resulting in a total enhancement of 22.4/17.5 K (Fig.14).
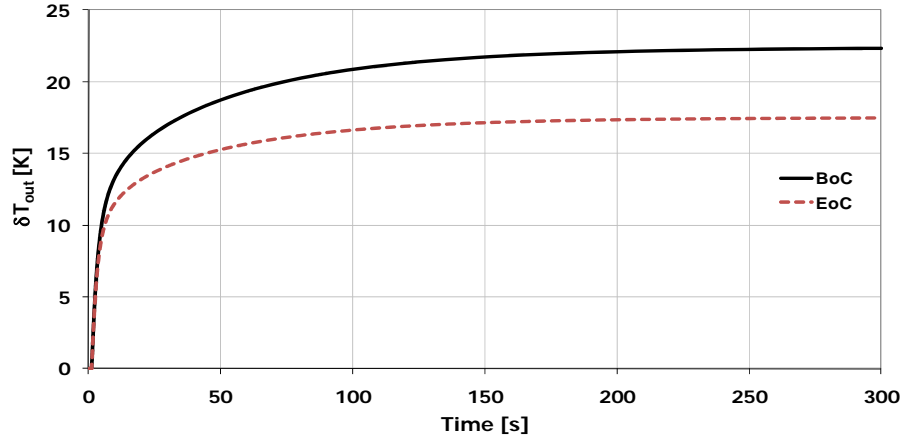
Fig. 14. Core outlet temperature variation following a step reactivity insertion of 50 pcm.

By applying the energy balance on the whole core at BoC:

$$q = \Gamma C_l (T_{out} - T_{in}) = 2575 \cdot 71456 \cdot (502.4 - 400) = 3840 MW \tag{25}$$

and EoC

$$q = \Gamma C_l (T_{out} - T_{in}) = 2575 \cdot 71456 \cdot (497.5 - 400) = 3656 MW, \tag{26}$$

it has been observed that the model predictions overestimate the power transferred to coolant of about 12.6 and 9.9 MW$_{th}$ respectively, which have been judged as well acceptable results.

Analysis of the impact of not-linked axial expansion and average coolant temperature radial expansion

The reference model (22) has been modified so as to specifically allow the demonstration of the impact of different phenomena during BoC and EoC transients.

In particular, the reactivity feedback calculations have been modified to be based on the average fuel and coolant temperatures rather than cladding average and coolant inlet temperatures, respectively.

The first modification has been required to assess the impact of assuming the pellet column to be not-linked to the cladding –and consequently the axial expansion to be controlled by the fuel temperature, as expressed in Eq. (14); the latter has been applied in order to evaluate the effect of considering the core radial expansion to be driven by the coolant average temperature, pursuant to Eq. (15).

In ANNEX A the main input parameters and results pertaining to such analyses have been accounted for what concerns parameters subject to the most restricting technological constraints, namely fuel and superficial cladding temperatures.

In the case of core inlet temperature enhancement, no significant differences from the reference simulations have been generally found. In particular, the fuel average temperature asymptotic variation has turned out to range from – 67 K (not-linked configuration, core inlet temperature radial expansion) to - 44 K (linked configuration, lead average temperature radial expansion) at BoC, and from – 45 K (linked configuration, core average temperature radial expansion) to - 24 K (not-linked configuration, lead average temperature radial expansion) at EoC.

The cladding average temperature excursion varies from a minimum of + 4.44 K (linked configuration, lead average temperature radial expansion) to a maximum of + 5.35 K (not-linked configuration, lead average temperature radial expansion) at BoC, and from a minimum of + 7.46 K (not-linked configuration, core inlet temperature radial expansion) to a maximum of + 7.78 K (linked configuration, lead average temperature radial expansion) at EoC, the corresponding reference values being + 3.44 K and + 3.54 K respectively.

As to power level, asymptotic variations from the steady-state values spread from – 18.3 MW_{th} (not-linked configuration, core inlet temperature radial expansion) to – 15.8 MW_{th} (not-linked configuration, lead average temperature radial expansion) at BoC, and from – 19.2 MW_{th} (linked configuration, lead average temperature radial expansion) to - 8.2 MW_{th} (not-linked configuration, lead average temperature radial expansion) at EoC.

In the case of a step reactivity insertion of 50 pcm, the fuel average temperature asymptotic variation has turned out to range from + 230 K (linked configuration, lead average temperature radial expansion) to + 339 K (not-linked configuration, core inlet temperature radial expansion) at BoC, and from + 118 K (not-linked configuration, core average temperature radial expansion) to + 189 K (linked configuration, lead average temperature radial expansion) at EoC.

The cladding average temperature excursion varies from a minimum of + 20.1 K (not-linked configuration, lead average temperature radial expansion) to a maximum of + 23.6 K (linked configuration, lead average temperature radial expansion) at BoC, and from a minimum of + 8.2 K (not-linked configuration, lead average temperature radial expansion) to a maximum of + 19 K (linked configuration, lead average temperature radial expansion) at EoC, the corresponding reference values being + 28 K and + 22 K respectively.

As to power level, asymptotic variations from the steady-state values spread from + 68 MW_{th} (not-linked configuration, lead average temperature radial expansion) to + 80 MW_{th} (not-linked configuration, core inlet temperature radial expansion) at BoC, and from + 28 MW_{th} (not-linked configuration, lead average temperature radial expansion) to + 65 MW_{th} (linked configuration, lead average temperature radial expansion) at EoC, pointing a large variability out.

2.5   DEMO core open loop stability

Stability and natural response characteristics of the continuous-time LTI system (i.e., linear with matrices that are constant with respect to time) described in Eq. (22) have been also investigated directly by means of its representative transfer function, which has been obtained by Laplace-transforming the state-space model itself in MATLAB. The matrix-valued transfer function:

$$G(s) = \frac{Y(s)}{U(s)} \tag{27}$$

provides indeed qualitative insights into the response characteristics of the system, being stability very easy to infer from the related pole-zero plot: in order for a linear system to be stable, in fact, all of its poles (namely, roots of the characteristic equation or, equivalently, eigenvalues of the matrix $\underline{\underline{A}}$) must have negative real parts, that is they must all lie within the left-half of the s-plane [19].

TABLE IV

Pole location.

Pole	Value at BoC [s^{-1}]	Value at EoC [s^{-1}]
P_1	- 0.0188	- 0.0120
P_2	- 0.0201	- 0.0214
P_3	- 0.0785	- 0.0801
P_4	- 0.199	- 0.208
P_5	- 0.561 + 0.125i	- 0.580 + 0.136i
P_6	- 0.561 - 0.125i	- 0.580 - 0.136i
P_7	- 2.48	- 2.47
P_8	- 6.58	- 6.54
P_9	- 27.1	- 27.0
P_{10}	$-3.96 \cdot 10^3$	$-3.80 \cdot 10^3$

As a result of such an investigation, the system has been confirmed to be stable at both BoC and EoC, since all its ten poles have strictly negative real part, the dominant ones being at - 0.0188 and - 0.0120 s^{-1}, respectively (see Table IV).

3   NEUTRON KINETICS EVALUATIONS

To extend the previous DEMO neutronics analyses by investigating core responses to transient initiators such as temperature changes or control rod shifts, a preliminary study of DEMO core kinetics has been carried out. Indeed, kinetics studies are fundamental not only to predict the reactor behaviour under operational conditions, but also to evaluate consequences of hypothetical accidents for safety purposes.

In this context, the ERANOS KIN3D module [10] has been employed to accomplish simulations of reactor transients induced by both fuel temperature (Doppler effect) and coolant temperature (coolant density effect) variations, and a FAR complete withdrawal and insertion.

To perform such analyses, the perturbations related to the reactivity effects under investigation have been simulated by cross-section changes in some reactor sub-regions, based on the outcomes of the previous study of DEMO core dynamics concerning fuel and coolant temperature variations following a stepwise reactivity insertion of 50 pcm and an increase of the coolant inlet temperature of 10 K. Material density and temperature distributions obtained from the previous coupled point-kinetics and thermal-hydraulics model have been employed to compute effective neutron cross-sections for reactor sub-regions that have been used as input data for the present core neutronics calculations.

Reactivity coefficients and kinetics parameters, such as β_{eff}, have been calculated accordingly by employing the perturbation theory formalism for the steady-state conditions, in order to assess both reactivity global variations and their breakdown into the most relevant nuclide contributions.

KIN3D point and direct space-time kinetics solution schemes have been finally analyzed and compared, with the purpose to test the code capabilities in view of more complex transient evaluations to be performed in the future.

3.1   Computational schemes

Multi-group cross-sections associated to every reactor zone have been processed by means of ECCO and tri-dimensional core models have been set up. The whole system has then been solved through both the variational nodal (transport and diffusion options) and finite-difference (diffusion) methods, in order to evaluate their impact on the solution accuracy. For the same purpose, nodal transport calculations have been performed using either spherical harmonics (P_N) and simplified spherical harmonics (SP_N), while representing the scattering cross-sections with the P_0 and P_1 Legendre polynomial expansion (P_3P_0, P_3P_1, SP_3P_0, SP_3P_1 respectively).

Regarding KIN3D, the module solves the time-dependent neutron transport equation and performs perturbation calculations. The treatment of the time dependence is based on two main models: point and space-time kinetics.

In point kinetics, the flux shape (that determines the power shape and reactivity coefficients) is assumed to be constant during the transient, the reactor being considered to be in steady state mode for $t < 0$, and being $t = 0$ the beginning of a transient.

Concerning the space-time kinetics calculations, the time-dependent problem is transformed into a sequence of steady-state-like problems, solved by VARIANT every time step, whereas cross-sections are assumed to be known at certain times during the transient (e.g. FAR position at initial and final state), and an interpolation between these time points is performed. Two main space-time kinetics methods have been tested: the direct method and the quasi-static space-time factorisation scheme.

The first uses a straightforward time discretization of the time-dependent neutron transport (or diffusion) equation, featuring a relative simplicity –since there is no need for perturbation theory calculations which require computation of the adjoint steady-state flux-, but a quite relevant computing cost, as it has been found that the method requires extremely fine time steps for transient simulations in fast reactors due to considerably small values of the mean generation time ($\Lambda \sim 8.2 \cdot 10^{-7}$ s, DEMO BoC reference calculations).

The second is based on the observation that the flux shape does not have to be updated as frequently as the flux amplitude, which represents a rapidly varying factor that is calculated with small time steps by employing the point kinetics integration scheme. Flux shape updates provide new power distributions and new sets of reactivity coefficients, showing good performances without any significant loss of accuracy. The equations, however, are more complicated than those of the direct method, adjoint and perturbation theory calculations being necessary.

3.2   Results

KIN3D has been employed to perform simulations of DEMO core transients induced by fuel and coolant temperature variations, and FAR complete withdrawal and insertion.

Consistently with the final steady-state temperature distributions resulting from the dynamics simulations performed, where the transients originated from a stepwise reactivity insertion of 50 pcm and an increase of the coolant inlet temperature of 10 K, deviations from the nominal parameters have been applied as follows:

- fuel temperature increase (variation: + 276 K);

- fuel temperature reduction (variation: - 54 K);

- coolant density reduction (maximum variation: - 0.13 %).

In point-kinetics calculations, the respective perturbations have been introduced at time $0 \leq t \leq 76$ s, and simulations were run for 500 s with a time step $\Delta t = 0.5$ s for $0 \leq t \leq 100$ s, and $\Delta t = 5$ s from for $100 \leq t \leq 500$ s.

Furthermore, one of the 16 regulation FARs (uniformly inserted to half active height at BoC) has been simulated to be either completely extracted from the core or totally pulled down, by figuring a speed of approximately 0.3 m s^{-1}. Perturbations have been introduced at time $t = 1$ s, and simulations were run for 10 s with a time step $\Delta t = 0.01$ s for $0 \leq t \leq 1.5$ s, and $\Delta t = 0.1$ s for $1.5 \leq t \leq 10$ s.

Fuel temperature variation

The calculated KIN3D reactivity variation due to an increase of 276 K in the fuel average temperature has turned out to be of the order of -50 pcm, showing a very good agreement (1.8 % discrepancy on $\Delta\rho$) with the direct P_3P_0 transport calculations performed in (§ 2).

As shown in Fig. 15, a perfect accordance (0.06 % discrepancy) has been found also between SP_3P_0 transport and diffusion calculations, whose results are $\Delta\rho = -49.75$ pcm and $\Delta\rho = -49.78$ pcm respectively, despite a 600 pcm maximum discrepancy on the corresponding absolute values of k_{eff}. Indeed, systematic errors in over-estimating or under-estimating k_{eff} actual values occur both in the reference and in the perturbed calculations, and differentials result less sensitive to numerical schemes as consequence of such 'first order' compensations.

Similarly, a reactivity increase ($\Delta\rho = +10.9$ pcm) has been induced by a 54 K reduction of the fuel average temperature. This smaller effect has been consistently determined in diffusion and transport calculations, the obtained results differing by only 0.06 %.
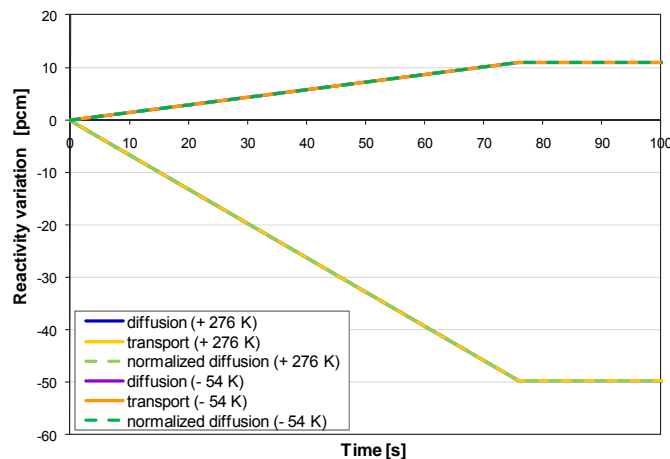
Fig. 15. Reactivity variations due to fuel temperature changes (KIN3D point-kinetics calculations).

Satisfactory results have been achieved with regard to the amplitude function curves as well: as depicted in Fig. 16, the exponentially soaring and dimming-to-zero trends refer to the positive and negative reactivity insertions, respectively.

Negligible disagreements between SP_3P_0 transport and diffusion calculations have been obtained, the maximum gap turning out to be of the order of 0.4 %.

Point-kinetics results have been then compared to the reference space-time direct results, and a 2 % discrepancy on the amplitude function has been found.
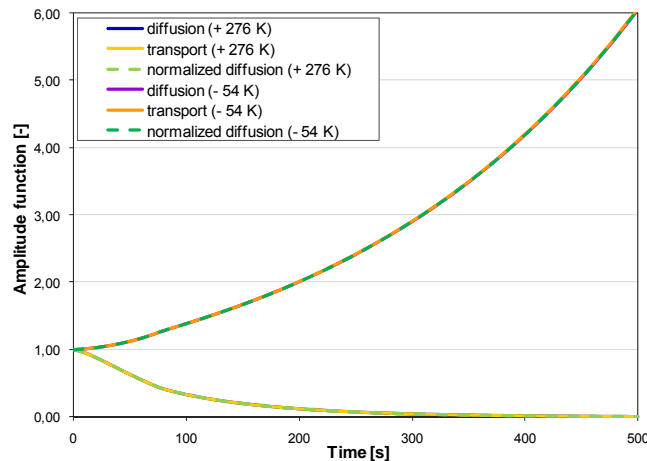
Fig. 16. Amplitude functions following fuel temperature changes (KIN3D point-kinetics calculations).

In order to test the KIN3D quasi-static space-time factorization scheme, a shorter transient has been simulated, due to the need of reducing the time step to make it comparable to the mean generation time. The resulting reactivity and amplitude have been compared to the point-kinetics results: a 0.7 % and 0.2 % discrepancy has been found for the respective figures. Additionally, the reactivity effect for the reference scenario (+ 276 K fuel temperature variation) has been decomposed reaction-wise, isotope-wise, and energy-group-wise, the breakdown being performed by means of the ERANOS PERTURBATION modules.

As summarized in Tab. V, the reaction-wise decomposition has shown that the dominant negative effect is due to capture, whereas fission gives a positive contribution. More specifically, the ^{238}U increased captures are responsible up to 91% of the total reactivity decrease; a negative effect is also due to ^{240}Pu and ^{239}Pu capture, but the strong compensation between the latter's capture and fission ends up with a slight positive net contribution.

First-order perturbation calculations (employing direct and adjoint finite-difference diffusion fluxes) have turned out to be in good agreement with KIN3D (variational nodal diffusion and transport) results concerning the global reactivity effect, which has been satisfactorily assessed with a 0.9 % discrepancy.

TABLE V

Doppler reactivity effect breaking-down by nuclides and reactions.

Isotope	Capture	Fission	Leakage	Elastic Removal	Inelastic Removal	*n,xn* Removal	TOTAL
Cr53	0.00	0.00	0.00	-0.01	0.00	0.00	-0.01
Fe56	-0.27	0.00	0.00	-0.03	0.00	0.00	-0.30
Mo96	0.01	0.00	0.00	0.00	0.00	0.00	0.01
Pb204	-0.01	0.00	0.00	0.00	0.00	0.00	-0.01
Pb206	-0.03	0.00	0.00	-0.01	0.00	0.00	-0.03
Pb207	-0.06	0.00	0.00	-0.01	0.00	0.00	-0.07
Pb208	0.00	0.00	0.00	-0.02	0.00	0.00	-0.02
U238	-45.73	0.01	0.32	0.05	-0.10	0.00	-45.46
Pu238	-0.03	-0.03	0.00	0.00	0.00	0.00	-0.06
Pu239	-5.53	7.52	-0.11	0.00	0.00	0.00	1.87

Pu240	-4.14	0.45	-0.06	0.00	0.00	0.00	-3.75
Pu241	0.03	-1.54	-0.01	0.00	0.00	0.00	-1.51
Pu242	-0.25	0.00	-0.01	0.00	0.00	0.00	-0.25
B10	-0.50	0.00	0.00	0.00	0.00	0.00	-0.50
O16	0.00	0.00	0.00	-0.12	0.00	0.00	-0.12
TOTAL	-56.50	6.41	0.14	-0.15	-0.10	0.00	-50.20

Coolant density variation

The calculated KIN3D reactivity variation due to an increase of 11 K in the coolant average temperature has turned out to be of the order of - 16 pcm. As shown in Fig. 17, a fairly good agreement (5.6 % discrepancy) has been found between SP_3P_0 transport and diffusion calculations, whose results are $\Delta\rho = + 16.05$ pcm and $\Delta\rho = +15.14$ pcm respectively.
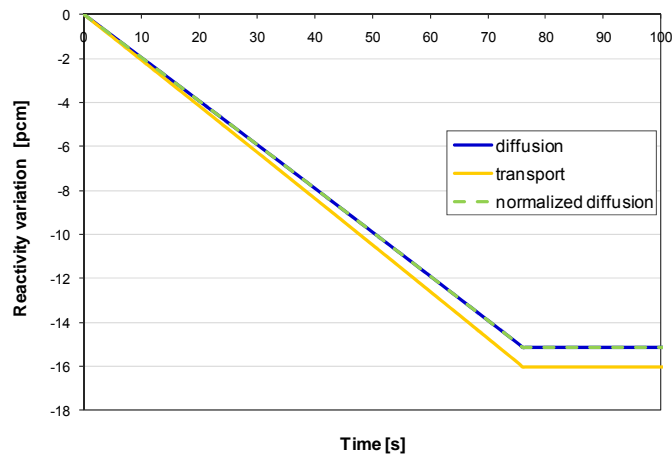
Fig. 17. Reactivity variations due to coolant temperature increase by 11 K (KIN3D point-kinetics calculations).

Quite reasonable accordance has been achieved in determining the respective amplitude functions: as depicted in Fig. 18 in fact, the diffusion exponential dimming-to-zero trends show a 11 % disagreement with respect to the SP_3P_0 transport outcome.
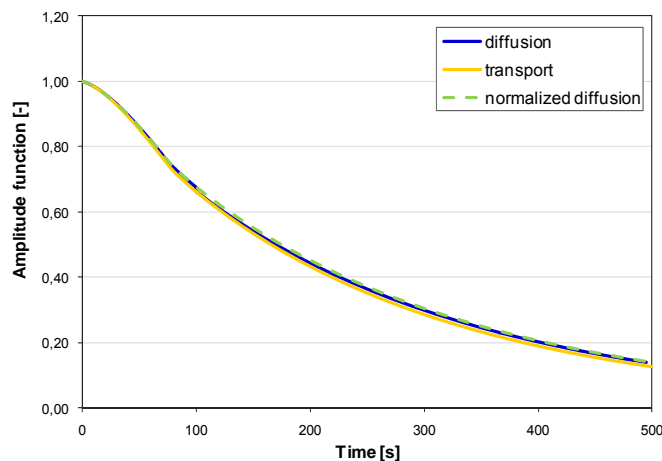
Fig. 18. Amplitude functions following a coolant temperature increase by 11 K (KIN3D point-kinetics calculations).

As in the Doppler effect case, the global reactivity variation has been broken down reaction-wise, isotope-wise, and energy-group-wise. First-order perturbation calculations have turned out to be in fair agreement with KIN3D results concerning the global reactivity effect, which has been assessed with a 13 % discrepancy.

As summarized in Tab. VI, the reaction-wise decomposition has shown that the negative effect is mostly due to leakage, which accounts for about - 23 pcm and, as expected, is almost entirely due to the lead, whereas capture, elastic and inelastic removals oppose the reactivity diminution.

Regarding the fuel most relevant nuclides, ^{238}U has confirmed to contribute positively since even-even isotope capture cross-sections decrease, due to the spectral hardening following a coolant density reduction.

Absolute values of k_{eff} have been finally determined with approximately 60 pcm difference between P_3P_0 and SP_3P_0 transport methods, and with approximately 550 pcm gap between SP_3P_0 transport and diffusion calculations.

TABLE VI

Doppler reactivity effect breaking-down by nuclides and reactions.

Isotope	Capture	Fission	Leakage	Elastic Removal	Inelastic Removal	*n,xn* Removal	TOTAL
C0	0.00	0.00	-0.01	0.00	0.00	0.00	-0.01
Cr52	0.00	0.00	-0.02	0.01	0.00	0.00	-0.01
Fe56	0.11	0.00	-0.25	0.11	0.01	0.00	-0.02
Mo95	0.01	0.00	0.00	0.00	0.00	0.00	0.01
U238	0.19	-0.03	-0.02	0.00	0.03	0.00	0.18
Pu239	0.03	-0.12	0.00	0.00	0.00	0.00	-0.09
Pu240	0.02	-0.01	0.00	0.00	0.00	0.00	0.01
Pu241	0.00	-0.01	0.00	0.00	0.00	0.00	-0.01
B10	-0.13	0.00	-0.01	0.00	0.00	0.00	-0.14
B11	0.00	0.00	-0.02	0.00	0.00	0.00	-0.01
O16	0.00	0.00	-0.04	0.06	0.00	0.00	0.02
Pb204	0.40	0.00	-0.36	0.05	0.14	0.00	0.23
Pb206	0.93	0.00	-5.18	0.67	2.05	-0.01	-1.53
Pb207	0.59	0.00	-5.10	0.78	1.46	-0.03	-2.31
Pb208	0.16	0.00	-11.96	1.46	0.92	-0.05	-9.47
TOTAL	2.33	-0.16	-22.98	3.14	4.62	-0.09	-13.15

Control element shifting

KIN3D has been finally employed to simulate a transient initiated by either a FAR complete extraction or its total insertion from/into the core.

The corresponding reactivity variations have turned out to be of the order of $\Delta\rho = + 320$ pcm (see Fig. 19) and $\Delta\rho = - 550$ pcm, the latter effect being greater because of the weaker self-shielding in the bottom part of the active core. A very good agreement (1.2 % and 0.5 % discrepancies) has been found also between SP_3P_0 transport and diffusion calculations, resulting respectively in $\Delta\rho = + 318$ pcm and $\Delta\rho = + 322$ pcm in the case of rod withdrawal, and in $\Delta\rho = - 554$ pcm and $\Delta\rho = - 552$ pcm in the case of rod insertion.

As in the previous cases, the global reactivity variation following the reference perturbation (i.e. FAR complete extraction) has been decomposed into its main contributors (see Tab. VII) by applying the first-order perturbation theory. Results have turned out to be in fair agreement with KIN3D results concerning the global reactivity effect, which has been assessed with a 14 % maximum discrepancy.

The reaction-wise decomposition has shown that the positive effect is predominantly due to the significant reduction of captures in the FA deprived of absorbers, accounting for about 354 pcm, 350 of which are due to ^{10}B; a minor positive contribution (+ 30 pcm) is also due to ^{10}B and ^{11}B elastic removal.
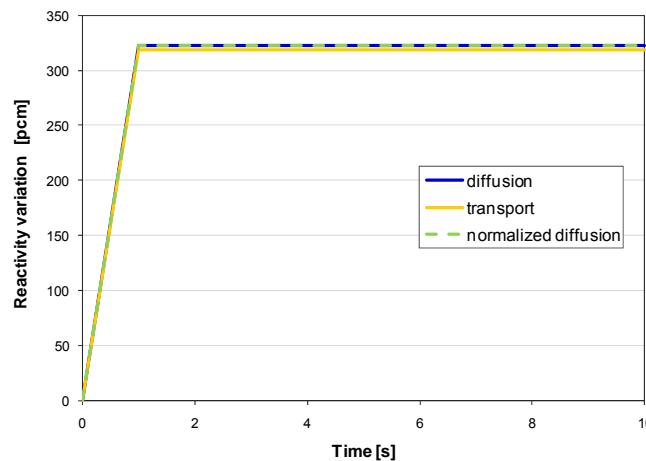
Fig. 19. Reactivity variation due to a FAR complete withdrawal from the active core (KIN3D point-kinetics calculations).

TABLE VI

FAR withdrawal reactivity effect breaking-down by nuclides and reactions.

Isotope	Capture	Fission	Transport	Elastic Removal	Inelastic Removal	*n,xn* Removal	TOTAL
C0	-0,01	0,00	0,78	-2,05	-0,01	0,00	-1,29
Si28	0,00	0,00	0,00	0,00	0,00	0,00	0,01
Cr52	0,00	0,00	0,03	0,01	0,00	0,00	0,05
Cr50	0,00	0,00	0,00	0,01	0,00	0,00	0,01
Cr53	0,00	0,00	0,01	0,01	0,00	0,00	0,02
Mn55	0,00	0,00	0,00	0,00	0,00	0,00	0,01
Fe54	0,01	0,00	0,03	0,01	0,00	0,00	0,05
Fe56	0,11	0,00	0,12	0,19	0,02	0,00	0,45
Fe57	0,00	0,00	0,02	0,00	0,00	0,00	0,02
U235	0,01	-0,13	0,00	0,00	0,00	0,00	-0,11
U238	2,23	-0,70	-1,33	0,07	0,66	-0,01	0,92
Pu238	0,03	-0,28	-0,01	0,00	0,00	0,00	-0,26
Pu239	0,78	-10,03	-0,31	0,01	0,08	0,00	-9,47
Pu240	0,41	-1,09	-0,16	0,01	0,05	0,00	-0,78
Pu241	0,09	-1,50	-0,03	0,00	0,01	0,00	-1,44
Pu242	0,11	-0,21	-0,05	0,00	0,02	0,00	-0,12

Pb204	0,03	0,00	-0,07	0,01	0,01	0,00	-0,02
Pb206	0,06	0,00	-1,04	0,08	0,22	0,00	-0,69
Pb207	0,05	0,00	-1,04	0,08	0,15	0,00	-0,75
Pb208	0,02	0,00	-2,49	0,15	0,08	0,00	-2,24
Ar40	0,00	0,00	0,02	-0,01	0,00	0,00	0,01
O16	0,03	0,00	-1,59	1,48	0,00	0,00	-0,07
B10	350,49	0,00	-3,62	12,21	0,10	0,00	359,18
B11	0,01	0,00	-4,12	18,35	0,10	0,00	14,34
TOTAL	354,47	-13,94	-14,82	30,63	1,51	-0,02	357,83

4   PRELIMINARY EVALUATIONS OF CORE MECHANICS-RELATED ASPECTS

The need of approaching mechanics-related aspects has led to an alternative and more simplified dynamic model of DEMO core. As in (§ 2), the primary system has been assumed to consist only in the active core, disregarding both upper and lower plena, and a single average channel representation has been adopted.

Reactor power has been described by neutron point-kinetics equations with six delayed neutron precursor groups.

An energy balance over the fuel pin surrounded by coolant -in which reactor power is an input retrieved from reactor kinetics- has been employed to determine the fuel and the lead temperature behaviour.

System expansions and contractions have been simulated under the simplifying hypothesis of considering a cylindrical-shape core, whose relative displacement vary instantaneously with temperature.

The so-calculated thermal-hydraulic and spatial parameters have been finally employed to insert the reactivity feedbacks into the neutronics equations (Fig. 20).
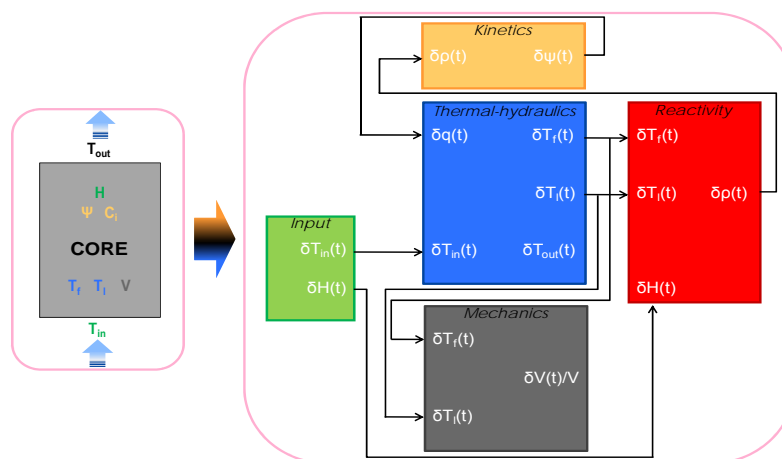
Fig. 20. DEMO core block scheme.

4.1 Mathematical model

Neutron Kinetics Equations

Concerning neutronics, it has been again assumed that neutron time fluctuations and spectrum are independent of spatial variations and neutron level, respectively. Accordingly, the core has been considered as a lumped source of neutrons with prompt heat power, with neutron population and neutron flux related by constants of proportionality, leading to the point-kinetics approximation to be employed (§ 2.3). Consequently, Eq. (9), (10), (11) and (12) have been employed.

Reactivity and Feedback Function

Consistently with the lumped parameter modelling employed, reactivity feedback has been expressed as a function of the mean values of both fuel and coolant temperature. Moreover, externally introduced reactivity has been simulated by the coefficient α_H associated with the insertion length of an ideal control rod, which has handled as a simple input parameter.

Under the hypotheses of small perturbations, the reactivity variation depends linearly on constant coefficients associated with the respective parameter variation from its steady-state value; therefore, continuous reactor feedbacks have been calculated as follows:

$$\delta\rho(t) = (\alpha_D + \alpha_E)\delta T_f + (\alpha_L + \alpha_E)\delta T_l + \alpha_H \delta H \tag{28}$$

In the above expression the first term in the right-hand side represents the feedback effects induced by changes of fuel temperature: in particular, the coefficient α_D accounts for the Doppler effect, whereas α_E represents the contribution concerning the core expansion due to fuel temperature raise. Analogously, the second term represents the feedbacks owing to the coolant, namely the effect of density and the share of core expansion pertaining to lead temperature variations. In fact, coherently with the zero-dimensional approach, reactivity oscillations induced by core dimensional changes have been taken into account by assuming that DEMO core expands homogeneously depending on an average temperature value as follows:

$$\delta\rho(t)\big|_{\exp} = \alpha_V \frac{dV(t)}{V} = \alpha_V B \frac{\delta T_f(t) + \delta T_l(t)}{2} = \alpha_E\big(\delta T_f(t) + \delta T_l(t)\big), \tag{29}$$

where the total volumetric expansion coefficient B has been properly evaluated on the basis of both the steel- and fuel-related values in correspondence to the respective theoretical mean temperatures at steady-state, and α_V has been calculated as:

$$\alpha_V = \frac{\partial\rho}{\partial\left(\dfrac{dV}{V}\right)} = \frac{\alpha_R + \alpha_Z}{3} \tag{30}$$

with:

$$\alpha_R = \frac{\partial \rho}{\partial \left(\dfrac{dR}{R} \right)} ; \quad \alpha_Z = \frac{\partial \rho}{\partial \left(\dfrac{dZ}{Z} \right)} . \tag{31}$$

Thermal-hydraulics Equations

The equations below describe the single node transient behaviour of fuel and coolant temperatures in the active core region.

For the gradient of the average fuel temperature, the heat transfer process has been achieved by taking an energy balance over an ideal fuel element surrounded by coolant:

$$M_f C_f \frac{dT_f(t)}{dt} = q(t) - U(T_f(t) - T_l(t)) , \tag{32}$$

where:

- properties and thermal resistances of fuel, gap and cladding have been assumed constant with temperature and time;
- the global heat transfer coefficient U, describing a combined heat transfer coefficient from fuel to lead bulk, has been calculated in correspondence to the average nominal temperatures and kept constant throughout the dynamic analysis;
- conduction in the axial direction has been neglected;
- the power generated in the fuel by fission has been obtained from neutron kinetics equations (according to the relation $n(t)/n_0 = q(t)/q_0$) and has been treated as an input for the heat transfer dynamic model.

The energy balance equation for the coolant, by using the symmetrical definition of $T_l = (T_{in} + T_{out})/2$ in which the lead inlet temperature is an input variable, has been written as:

$$M_l C_l \frac{dT_l(t)}{dt} = U(T_f(t) - T_l(t)) - \Gamma C_l (2T_l(t) - 2T_{in}(t)) . \tag{33}$$

Eq. (32) and (33) have been perturbed around the steady-state and linearized in turn, leading to:

$$\frac{d\delta T_f(t)}{dt} = -\frac{1}{\tau_f} \delta T_f(t) + \frac{1}{\tau_f} \delta T_l(t) + \frac{q_0}{M_f C_f} \delta \psi(t) \tag{34}$$

and

$$\frac{d\delta T_l(t)}{dt} = \frac{1}{\tau_l} \delta T_f(t) + \left(-\frac{1}{\tau_l} - \frac{2}{\tau_0} \right) \delta T_l(t) + \frac{2}{\tau_0} \delta T_{in}(t) , \tag{35}$$

with time constants $\tau_f = (M_f C_f)/U$, $\tau_l = (M_l C_l)/U$, and $\tau_0 = M_l/\Gamma$.

Mechanical Response Equation

Core dimensional variations have been derived under the assumption that displacements depend instantaneously on temperature rise. The equation describing the time dependence of the relative volumetric expansion has been derived as a function of the fuel/coolant-averaged temperature multiplied by B, which has been assumed to be temperature and time independent, as Eq. (13) indicates:

$$\frac{\delta V}{V}(t) = \mathrm{B}\,\frac{\left(\delta T_f(t) + \delta T_l(t)\right)}{2}. \tag{36}$$

4.2   Simulations and results

The modelling equations described above have been handled in terms of state vector ($\underline{X}$), input vector ($\underline{U}$), output vector ($\underline{Y}$), corresponding matrices ($\underline{A}$, $\underline{B}$ and $\underline{C}$ respectively) and feed-through matrix $\underline{D}$.

The corresponding MIMO (Multi Input – Multi Output) system described by has been directly simulated in MATLAB, once the four matrices have been obtained.

It presents nine state variables: (namely, variations of fuel temperature, coolant average temperature, neutron population, and neutron precursors), two inputs (namely, variations of lead inlet temperature and control rod extraction length) and eight outputs (namely, variations of: fuel temperature, coolant average and outlet temperature, core mean temperature, neutron population, reactivity, core relative displacement and power):

$$
\underline{A}=
\begin{bmatrix}
-\dfrac{1}{\tau_f} & \dfrac{1}{\tau_f} & \dfrac{q_0}{M_f C_f} & 0 & 0 & 0 & 0 & 0 & 0 \\
\dfrac{1}{\tau_l} & -\dfrac{1}{\tau_l}-\dfrac{2}{\tau_0} & 0 & 0 & 0 & 0 & 0 & 0 & 0 \\
\dfrac{(\alpha_D+\alpha_E)}{\Lambda} & \dfrac{(\alpha_L+\alpha_E)}{\Lambda} & \dfrac{-\beta}{\Lambda} & \dfrac{\beta_1}{\Lambda} & \dfrac{\beta_2}{\Lambda} & \dfrac{\beta_3}{\Lambda} & \dfrac{\beta_4}{\Lambda} & \dfrac{\beta_5}{\Lambda} & \dfrac{\beta_6}{\Lambda} \\
0 & 0 & \lambda_1 & -\lambda_1 & 0 & 0 & 0 & 0 & 0 \\
0 & 0 & \lambda_2 & 0 & -\lambda_2 & 0 & 0 & 0 & 0 \\
0 & 0 & \lambda_3 & 0 & 0 & -\lambda_3 & 0 & 0 & 0 \\
0 & 0 & \lambda_4 & 0 & 0 & 0 & -\lambda_4 & 0 & 0 \\
0 & 0 & \lambda_5 & 0 & 0 & 0 & 0 & -\lambda_5 & 0 \\
0 & 0 & \lambda_6 & 0 & 0 & 0 & 0 & 0 & -\lambda_6
\end{bmatrix}
$$

$$
\underline{B}=
\begin{bmatrix}
0 & 0 \\
\dfrac{2}{\tau_0} & 0 \\
0 & \dfrac{\alpha_H}{\Lambda} \\
0 & 0 \\
0 & 0 \\
0 & 0 \\
0 & 0 \\
0 & 0 \\
0 & 0
\end{bmatrix}
$$

$$
\underline{C}=
\begin{bmatrix}
1 & 0 & 0 & 0 & 0 & 0 & 0 & 0 & 0 \\
0 & 1 & 0 & 0 & 0 & 0 & 0 & 0 & 0 \\
0 & 2 & 0 & 0 & 0 & 0 & 0 & 0 & 0 \\
\dfrac{1}{2} & \dfrac{1}{2} & 0 & 0 & 0 & 0 & 0 & 0 & 0 \\
0 & 0 & 1 & 0 & 0 & 0 & 0 & 0 & 0 \\
\alpha_D+\alpha_E & \alpha_L+\alpha_E & 0 & 0 & 0 & 0 & 0 & 0 & 0 \\
\dfrac{B}{2} & \dfrac{B}{2} & 0 & 0 & 0 & 0 & 0 & 0 & 0 \\
0 & 0 & q_0 & 0 & 0 & 0 & 0 & 0 & 0
\end{bmatrix}
$$

$$
\underline{D}=
\begin{bmatrix}
0 & 0 \\
0 & 0 \\
-1 & 0 \\
0 & 0 \\
0 & 0 \\
0 & \alpha_H \\
0 & 0 \\
0 & 0
\end{bmatrix}
$$

$$
\underline{X}=
\begin{bmatrix}
\delta T_f \\ \delta T_l \\ \delta\psi \\ \delta\eta_1 \\ \delta\eta_2 \\ \delta\eta_3 \\ \delta\eta_4 \\ \delta\eta_5 \\ \delta\eta_6
\end{bmatrix}
\qquad
\underline{Y}=
\begin{bmatrix}
\delta T_f \\ \delta T_l \\ \delta T_{out} \\ \delta T_{core} \\ \delta\psi \\ \delta\rho \\ \dfrac{\delta V}{V} \\ \delta q
\end{bmatrix}
\qquad
\underline{U}=
\begin{bmatrix}
\delta T_{in} \\ \delta H
\end{bmatrix}
\tag{37}
$$

Simulations have been performed basing on the preliminary DEMO configuration at Beginning of Life (BoL); full details on the referred reactor description can be found in [20].

In Tab.VI I the main input data are given.

TABLE VII

DEMO core reference data.

Quantity	Value	Units	Quantity	Value	Units
β_1	6.302	pcm	α	-207	pcm
β_2	72.59	pcm	α_D	-0.1559	pcm K^{-1}
β_3	35.05	pcm	α_H	141	pcm cm^{-1}
β_4	114.4	pcm	α_L	-0.2096	pcm K^{-1}
β_5	70.42	pcm	α_R	-0.7153	-
β_6	22.52	pcm	α_Z	0.0785	-
λ_1	0.0125	s^{-1}	B	$3.7 \cdot 10^{-5}$	K^{-1}
λ_2	0.0292	s^{-1}	τ_f	3.12	s
λ_3	0.0890	s^{-1}	τ_l	3.34	s
λ_4	0.2557	s^{-1}	τ_0	0.21	s
λ_5	0.5946	s^{-1}	M_f	2391	kg
λ_6	2.6510	s^{-1}	C_f	317.5	J Kg^{-1} K^{-1}
Λ	$7.203 \cdot 10^{-7}$	s	q_0	$300 \cdot 10^6$	W
β	321	pcm			

Input parameters have been perturbed in order to investigate the open loop dynamic behaviour of DEMO core, as well as to observe the new equilibrium configuration reached after the transient.

In particular, the effects of lead inlet temperature increase (+1 K compared to its nominal value), and of an ideal control rod extraction (1 cm, corresponding to a reactivity step of 141 pcm) have been analyzed separately.

Lead Inlet Temperature Perturbation

The core inlet temperature has been enhanced by 1 K.

An increase of the average lead temperature -impacting both lead density and lead-temperature-driven expansion feedbacks- occurs (Figs. 21 and 22), leading to an insertion of negative reactivity (Fig. 23).
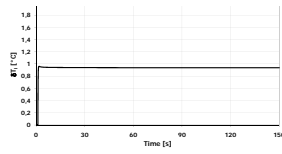
Fig. 21. Lead average temperature variation following an enhancement by 1 K of core inlet temperature.
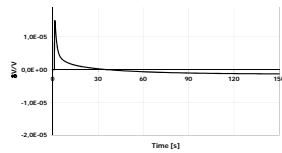
Fig. 22. Core volume relative displacement following an enhancement by 1 K of core inlet temperature.
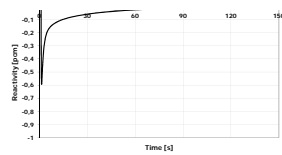
Fig. 23. Core reactivity variation following an enhancement by 1 K of core inlet temperature.

Because of the negative reactivity injection brought by higher lead temperatures, the core power undergoes a prompt decrease -showing a negative peak in the first part of the transient- (Fig. 24) as far as the fuel average temperature

reduction balances the increased lead temperature effects on reactivity thanks to the contributions of Doppler and fuel-temperature-driven expansion feedbacks (Fig. 25).

Correspondingly, the reactivity increases again showing first a rapid rise and then a slower slope due to the opposing contribution of coolant temperature feedbacks. Therefore, after a negative excursion of 0.6 MW$_{th}$, the reactor power rises so as to stabilize to a new equilibrium value, 0.47 MW$_{th}$ lower than the nominal one.
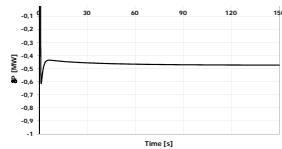
Fig. 24. Reactor power variation following an enhancement by 1 K of core inlet temperature.
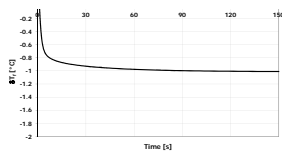
Fig. 25. Fuel average temperature variation following an enhancement by 1 K of core inlet temperature.

At the end of the transient, the lead outlet temperature shows a positive variation (+0.88 K), as Fig. 26 illustrates, but smaller than both the inlet perturbation and the average coolant temperature enhancement (+0.94 K), due to the decrease in reactor power outlined in Fig. 24. On the contrary, the fuel temperature response is monotonically negative and settles at -1.01 K.

As to core dimensional changes, basically driven by core average temperature, the volume exhibits first a relative expansion of 1.5·10^{-5}, and then a reduction, eventually settling at a relative variation of -1.4·10^{-6} with respect to the steady state value.
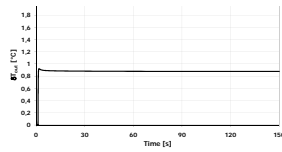
Fig. 26. Core outlet temperature variation following an enhancement by 1 K of core inlet temperature.

In order to verify the model prediction accuracy, the energy balance over the whole core has been calculated:

$$q = \Gamma C_l (T_{out} - T_{in}) = 25757 \cdot 1456 \cdot (480877 - 40\,1) = 29953\,MW \tag{38}$$

Looking at the model results, the reactor thermal power (Fig. 24) after transient is found to be 299.52 MW$_{th}$, hence the error committed using a linearized model is negligible.

Control Rod Extraction

A further perturbation has been performed in order to evaluate DEMO dynamic response to a step reactivity insertion of 141 pcm (Fig. 27).
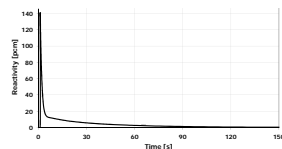
Fig. 27. Core reactivity variation following an externally given perturbation of 141 pcm.

As Fig. 28 highlights, the expected response is observed, i.e. the initial, instantaneous power rise (prompt jump), whose time characteristic (0.02 s) and huge amplitude (128 MW$_{th}$) are essentially determined by the prompt neutron life time and the delayed neutron fraction of the system, respectively.
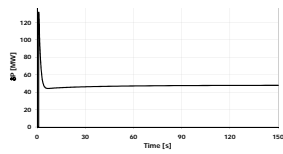
Fig. 28. Reactor power variation following a step reactivity insertion of 141 pcm.

After the power high peak at the transient beginning, fuel and lead temperatures (Figs. 29 and 30, respectively) start rising monotonically so as to balance the positive reactivity introduced by extracting the ideal control rod: finally, the corresponding negative reactivity feedbacks reduce the reactor power to a new stable value, 47.9 MW$_{th}$ higher than the nominal value.
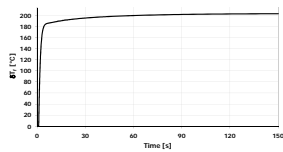
Fig. 29. Fuel average temperature variation following a step reactivity insertion of 141 pcm.
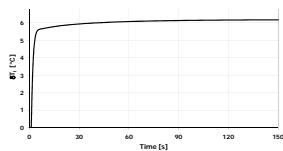
Figure 30. Lead average temperature variation following a step reactivity insertion of 141 pcm.

At the end of the transient, the fuel temperature variation results significantly positive, tending asymptotically to + 203 K.

As evident in Fig. 31, the average coolant temperature features in turn a positive variation of 6.19 K, and the lead outlet temperature shows an analogous trend but characterized by a major amplitude, resulting in a total enhancement of 12.4 K.
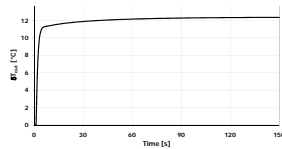
Fig. 31. Core outlet temperature variation following a step reactivity insertion of 141 pcm.

As to core dimensional changes, the total volume undergoes a relative expansion of $3.87 \cdot 10^{-3}$, following the core average temperature –and thus lead and fuel average temperatures- trend, as it is depicted in Fig. 32.
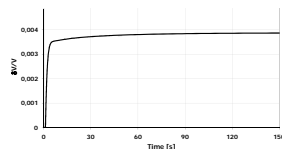
Fig. 32. Core relative displacement variation following a step reactivity insertion of 141 pcm.

By applying the energy balance on the whole core:

$$q = \Gamma C_l (T_{out} - T_{in}) = 257571456 \cdot (4924 - 400) = 34652 MW \tag{38}$$

it has been observed that the model predictions overestimate the power transferred to coolant of about 1.4 MW$_{th}$, which has been judged as a very satisfactory result.

4.3 DEMO core open loop stability

Stability and natural response characteristics of the continuous-time LTI system have been also investigated directly by means of its representative transfer function, which has been obtained by Laplace-transforming the state-space model itself in MATLAB.

As a result of such an investigation, the system has been confirmed to be stable, since all its nine poles (see Tab.VIII) have strictly negative real part, the dominant one being at -0.0124 s^{-1}. Furthermore, their location in the left half of the s-plane effectively define the system response components, in particular predicting an exponential decaying behaviour.

TABLE VIII

Pole location.

Pole	Value [s^{-1}]
P_1	0.0124
P_2	- 0.0271
P_3	- 0.0867
P_4	- 0.249
P_5	- 0.752
P_6	- 0.859
P_7	- 2.39
P_8	- 9.8
P_9	- 4.46·10^3

5 CONCLUSIONS

In the present work a preliminary analysis of DEMO primary system dynamic behaviour has been performed. The need of investigating reactor responses to temperature transients at BoC and EoC has led to a simplified model reckoning with all the main temperature-dependent reactivity feedback effects following a reactivity change.

Consequently, thermal-hydraulics and neutron kinetics have been studied through a simplified zero-dimensional linearized model -based on a small perturbation approach-, which have been handled in terms of state, input and output variables, so as to predict how the system reacts to a increase by 10 K of lead inlet and to the extraction of an ideal control rod, corresponding to a reactivity insertion of 50 pcm.

Results have shown the model is stable and evidences a satisfactory capability of predicting the response to both perturbations, since small errors have been figured.

An enhancement of 10 K in the lead inlet temperature has led to slight changes in reactor power and temperatures, the first settling at new equilibrium values 22.4/22.1 MW_{th} lower than the nominal ones (at BoC and EoC, respectively), and the latter exhibiting variations (negative for the average fuel temperature and positive for both cladding average temperature, and lead average and outlet temperatures) of some degrees.

As to the 50 pcm reactivity injection, a significant impact on core power and temperatures has been observed. In particular, the first has steadily increased by approximately 32 % (BoC) and 25 % (EoC) of its nominal value, leading to

a remarkable rise of fuel average temperature (of the order of 276 and 220 K, respectively). Lead average and outlet temperatures have undergone an enhancement of about 11 and 22 K (BoC), and 9 and 17 K (EoC), whereas the cladding temperatures have featured a significant relative positive variation of approximately 5 and 4 % correspondingly.

Further, the impact of assuming the pellet column to be not-linked to the cladding, and the radial expansion to be driven by the coolant average temperature has been evaluated, turning out to have a generally slight impact on the new equilibrium values of output variables after the transients.

The stable behaviour of the system have been pointed out by the investigation of its representative transfer function with its poles, which have shown strictly negative real part, ranging from $-3.96 \cdot 10^3$ and $-3.80 \cdot 10^3$ s^{-1} (most rapidly decaying ones) to -0.0188 and -0.0120 s^{-1} (dominant ones).

In conclusion, the presented model has put up satisfactory results to what concerns the study of DEMO dynamic performances and transient responses at both BoC and EoC, having provided a useful tool able to allow a relatively quick, qualitative analysis of fundamental dynamics and stability aspects.

Concerning the neutron kinetics analyses performed in association with dynamics studies, as a general remark, a good agreement has been found among the different variational nodal methods and approximations (e.g. different Legendre polynomial expansion orders whether the transport option was selected) employed in KIN3D. Indeed, despite a spread of about 600 pcm in the absolute values of k_{eff}, differentials appear to be less sensitive to numerical options as consequence of a kind of compensation between systematic errors affecting each scheme.

In the case of fuel temperature increase, KIN3D point and direct space-time kinetics solution schemes have been analyzed and compared. Results have shown a good agreement with the direct calculations assumed as a reference. Additionally, as expected, it has been found that the point-kinetic model is computationally efficient and provides accurate results for small perturbations, i.e. when "true" time-dependent distributions of power and reactivity coefficients may be assumed to be close to their steady-state distributions. Nevertheless, for an accurate and numerically stable space-time simulation, it has been necessary to set extremely fine time steps, implying a significantly higher computational cost.

Reactivity coefficients and kinetics parameters have finally been calculated by employing the perturbation theory formalism for the steady-state conditions, in order to assess both reactivity global variations and their breakdown into the most relevant nuclide contributions. A good agreement with the KIN3D results has been found on the global reactivity worth, which has been assessed with a 13 % maximum discrepancy.

Concerning the investigation of DEMO core mechanics-related dynamic behaviour, thermal-hydraulics, neutron kinetics and mechanics have been studied through a simplified zero-dimensional linearized model -based on a small perturbation approach-, which have been handled in terms of state, input and output variables, so as to predict how the system reacts to a unitary increase of lead inlet and to a unitary extraction of an ideal control rod. Results have shown the model is stable and evidences a satisfactory capability of predicting the response to both perturbations, since negligible errors have been figured.

An enhancement of 1 K in the lead inlet temperature has led to slight changes in reactor power and temperatures, the first settling at a new equilibrium value 0.47 MW$_{th}$ lower than the nominal one, and the latter exhibiting variations (negative for the average fuel temperature and positive for lead average and outlet temperatures) of at most 1 K.

As to core dimensional changes, core volume eventually has dropped by $1.4 \cdot 10^{-6}$ (relative displacement) with respect to its steady state value.

As to the 141 pcm reactivity injection, a significant impact on core power and temperatures has been observed. In particular, after an instantaneous rise of nearly 50 %, the first has steadily increased by 15 % of its nominal value, leading to a remarkable rise of fuel average temperature (of the order of 200 K). Lead average and outlet temperatures have undergone an enhancement of about 6 and 12 K respectively, whereas the core volume has featured a relative positive displacement of approximately 4 ‰.

The stable exponential behaviour of the system have been pointed out by the investigation of its representative transfer function and pole-zero plot, which have shown real strictly negative poles, ranging from $4.46 \cdot 10^{3}$ (most rapidly decaying one) to -0.0124 (dominant one) s^{-1}.

In conclusion, the presented model has put up satisfactory results to what concerns the study of DEMO preliminary configuration dynamic performances and transient responses. A useful tool allowing a relatively quick, qualitative analysis of fundamental dynamics and stability aspects has been provided, setting the basis for the development of a more detailed and accurate model able to simulate the coupling of neutron kinetics, thermal-hydraulics and mechanics by taking also dimensional effects into account (namely, radial and axial power distributions, mass inertia influence on the elastic behaviour of core structures, etc.).

REFERENCES

The contents of this report have been published in the following papers:

▪ S. Bortot, A. Cammi, C. Artioli, P. Console Camprini, R. Ghazy, "A SIMPLIFIED MODEL FOR A PRELIMINARY STUDY OF THE DYNAMIC BEHAVIOUR OF A SMALL GEN IV LFR DEMO", In: *Proceedings of the 18th International Conference on Nuclear Engineering (ICONE18)*, Xi'an, China, May 17-21, 2010.

▪ S. Bortot, G. Aliberti, "APPLICATION OF THE ERANOS KIN3D MODULE FOR A GEN-IV LFR DEMO KINETICS ANALYSIS", In: *Proceedings of the European Nuclear Conference (ENC 2010)*, Barcelona, Spain, 30 May – 2 June, 2010.

▪ S. Bortot, A. Cammi, P. Console Camprini, C. Artioli, R. Ghazy, M.E. Ricotti, "TRANSIENT EVALUATION OF A GEN-IV LFR DEMONSTRATION PLANT THROUGH A LUMPED PARAMETER ANALYSIS OF COUPLED KINETICS AND THERMAL-HYDRAULICS", In: *Proceedings of the 2010 International Congress on Advances in Nuclear Power Plants (ICAPP '10)*, San Diego, CA, USA, June 13-17, 2010.

▪ S. Bortot, G. Aliberti, A. Cammi, "ON THE APPLICATION OF NEUTRON KINETICS MODELS FOR A SMALL LFR CORE TRANSIENT ANALYSES", In: *TRANSACTIONS of the American Nuclear Society*, *ANS Annual Meeting*, 2011 [submitted].

▪ S. Bortot, A. Cammi, C. Artioli, "DYNAMIC PERFORMANCE ASSESSMENT OF MOX AND METALLIC FUEL CORE OPTIONS FOR A GEN-IV LFR DEMONSRATOR", In: *Progress of Nuclear Energy*, 2010 [submitted].

NOMENCLATURE

C	Average specific heat at constant pressure	$[\text{J kg}^{-1}\text{K}^{-1}]$
f	Volume fraction [-]	
k_{fc}	Fuel-gap-cladding global heat transfer coefficient	$[\text{W K}^{-1}]$
h_{cl}	Clad-lead global heat transfer coefficient	$[\text{W K}^{-1}]$
l	Linear expansion coefficient $[\text{K}^{-1}]$	
L	Axial length [m]	
M	Total mass in the core [kg]	
n	Neutron density $[\text{m}^{-3}]$	
q	Thermal power [W]	
R	Core radial coordinate [m]	
s	Variable of the Laplace transform $[\text{s}^{-1}]$	
t	Time [s]	
T	Average temperature [K]	
U	Total heat transfer coefficient $[\text{W K}^{-1}]$	
v	Lead velocity $[\text{m s}^{-1}]$	
V	Core volume $[\text{m}^{3}]$	
Z	Core axial coordinate [m]	
α	Doppler constant [pcm]	
α_D	Doppler reactivity feedback coefficient $[\text{pcm K}^{-1}]$	
α_H	Control rod reactivity feedback coefficient $[\text{pcm cm}^{-1}]$	
α_L	Coolant density reactivity feedback coefficient $[\text{pcm K}^{-1}]$	
α_R	Radial expansion reactivity feedback coefficient $[\text{pcm K}^{-1}]$	
α_Z	Axial expansion reactivity feedback coefficient $[\text{pcm K}^{-1}]$	
β	Total delayed-neutron fraction [-]	
β_i	i^{th} precursor group delayed-neutron fraction [-]	
B	Volumetric thermal expansion coefficient $[\text{K}^{-1}]$	
$\delta\eta_i$	i^{th} precursor group dimensionless concentration variation from the steady-state [-]	
δH	Control rod extraction length [cm]	
$\delta\rho$	Reactivity variation from the steady-state [pcm]	
$\delta\psi$	Variation of the dimensionless neutron density from the steady-state [-]	
δT	Variation of average temperature from the steady-state [K]	
Γ	Mass flow rate $[\text{kg s}^{-1}]$	
η_i	i^{th} precursor group dimensionless concentration [-]	
Λ	Invariant neutron average lifetime [s]	
λ_i	i^{th} precursor group decay constant $[\text{s}^{-1}]$	
ρ	Reactivity [pcm]	
P	Density $[\text{kg m}^{-3}]$	

τ_0 Core lead circulation time constant [s]

τ_{c1} Fuel-cladding-related time constant [s]

τ_{c1} Cladding-lead-related time constant [s]

τ_f Fuel-related time constant [s]

τ_l Lead-related time constant [s]

ψ Dimensionless neutron density [-]

Subscripts

0   Steady state

c   Cladding

f   Fuel

in   Inlet

l   Lead

out   Outlet

BIBLIOGRAPHY

1. A Technology Roadmap for Generation IV Nuclear Energy Systems – GIF 002-00 (2002).

2. L. CINOTTI et al., "The Potential of the LFR and the ELSY Project", *Proceeding of the International Congress on Advances in Nuclear Power Plants (ICAPP 2007)*, Nice Acropolis, France (2007).

3. S. BORTOT et al., "Preliminary Core Characterization of a Generation IV Lead Fast Reactor DEMO: Goals, Design Rationales and Options", *En. Conv. and Management* (2010).

4. S. BORTOT et. al., "Conceptual Core Design of a Generation IV LFR Demonstration Plant", *Proceedings of PHYSOR 2010 – Advances in Reactor Physics to Power the Nuclear Renaissance*, Pittsburgh, Pennsylvania, USA (2010).

5. J. DUDERSTADT, L. J. HAMILTON, *Nuclear Reactor Analysis*, Wiley, New York (1976).

6. G. RIMPAULT et al., "The ERANOS code and data system for Fast Reactor neutronic analyses", *International Conference on the PHYSics Of Reactors 2002 (PHYSOR2002)*, Seoul, Korea, (2002).

7. Joint Evaluated File (JEF) project, "The JEFF-3.1 Nuclear Data Library", Technical Report JEFF Report 21, OECD/NEA (2006).

8. The MathWorks, Inc. (2007).

9. SIMULINK® software, The MathWorks, Inc. (2005).

10. A. RINEISKI, "KIN3D: Module de cinétique spatiale et de perturbations pour TGV2. A space time kinetics and perturbation theory module for TGV2", Technical Report NT SPRC-LEPH-9-203.

11. G. RIMPAULT, "Physics Documentation of Eranos: the Ecco Cell Code", Technical Report DER-SPRC-LEPh-97-001 (1997).

12. J. M. RUGGERI et al., "TGV: A Coarse Mesh 3 Dimensional Diffusion-transport Module for the CCRR/ERANOS Code System", Technical Report DRNR-SPCI-LEPh-93-209 (1993).

13. Handbook on Lead-bismuth Eutectic Alloy and Lead Properties, Materials Compatibility, Thermal-hydraulics and Technologies 2007 Edition, OECD NEA No. 6195, ISBN 978-92-64-99002-9 (2007).

14. M. SAROTTO et al., "ELSY Core Design, Static Dynamic and Safety Parameters with the Open Square FA", Technical Report Deliverable D8, EURATOM (2009).

15. R. THETFORD and V. SOBOLEV, "Recommended properties of fuel, cladding and coolant for EFIT pre-design", Deliverable 3.4 (Draft 0.4), IP EUROTRANS Contract n. FI6W-CT-2004-516520, DM3 AFTRA WP3.1 (2005).

16. J. J. CARABAJO et al., "A review of the thermophysical properties of MOX and UO_2 fuels", *Journal of Nuclear Materials*, **299**, pp. 181-198 (2001).

17. A. ZHUKOV et al., "Heat Transfer in Lead Cooled Fast Reactor (LCFR)". *Proceedings of the ARS'94 International Topical Meeting on Advanced Reactors Safety*, **1**, pp. 66-69, Pittsburgh, USA (1994).

18. D. L. HETRICK, *Dynamics of Nuclear Reactors*, American Nuclear Society, La Grange Park (1993).

19. K. OGATA, *Modern Control Engineering*, Prentice Hall (2009).

20. S. BORTOT *et al*., "Feedback Coefficients Evaluation for an Advanced LFR Demonstrative Reactor*", International Conference on Nuclear Energy for New Europe 2009 (NENE '09)*, Bled, Slovenia, September 14-17, 2009.

ANNEX A

TABLE A-1

DEMO core BoC and EoC non-reference input data.

BoC CONFIGURATION				
Quantity	Axial T_f Radial T_{in}	Axial T_c Radial T_l	Axial T_f Radial T_l	Units
α_R	- 0.8715	- 0.8861	- 0.8861	pcm K^{-1}
α_Z	0.0331	0.0088	0.0331	pcm K^{-1}
τ_f	2.97	1.94	2.97	s
τ_{c1}	1.33	0.87	1.33	s
τ_{c2}	0.06	0.06	0.06	s
τ_l	0.16	0.16	0.16	s
τ_0	0.21	0.21	0.21	s
EoC CONFIGURATION				
Quantity	Axial T_f Radial T_{in}	Axial T_c Radial T_l	Axial T_f Radial T_l	Units
α_R	- 0.9234	- 0.9389	- 0.9389	pcm K^{-1}
α_Z	- 0.1912	- 0.1949	- 0.1912	pcm K^{-1}
τ_f	2.97	1.99	2.97	s
τ_{c1}	1.33	0.89	1.33	s
τ_{c2}	0.06	0.06	0.06	s
τ_l	0.16	0.16	0.16	s
τ_0	0.21	0.21	0.21	s

A.1. LEAD INLET TEMPERATURE

PERTURBATION

Not-linked, T_{in} radial expansion
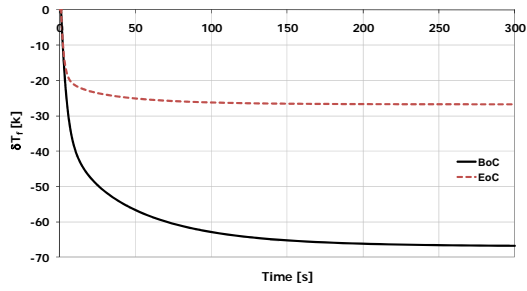
Fig. 1. Fuel average temperature variation following an enhancement by 10 K of core inlet temperature.
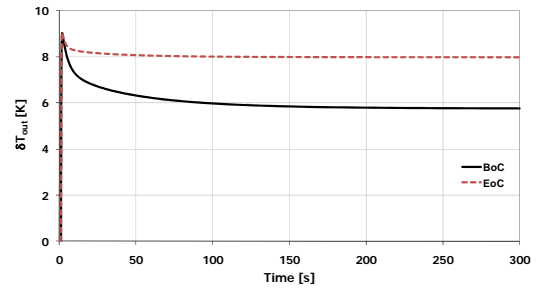
Fig. 2. Cladding average temperature variation following an enhancement by 10 K of core inlet temperature.
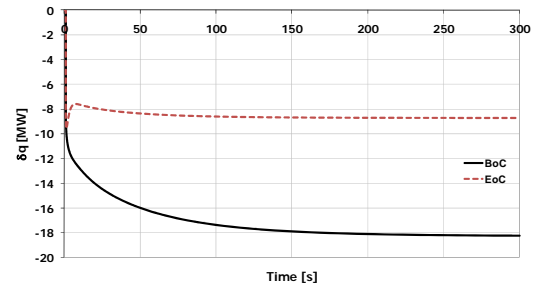
Fig. 3. Lead average temperature variation following an enhancement by 10 K of core inlet temperature.

Fig. 4. Core outlet temperature variation following an enhancement by 10 K of core inlet temperature.
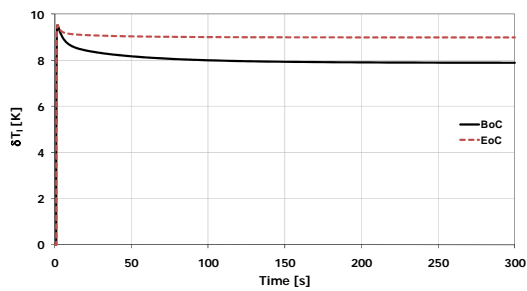
Fig. 5. Reactor power variation following an enhancement by 10 K of core inlet temperature.
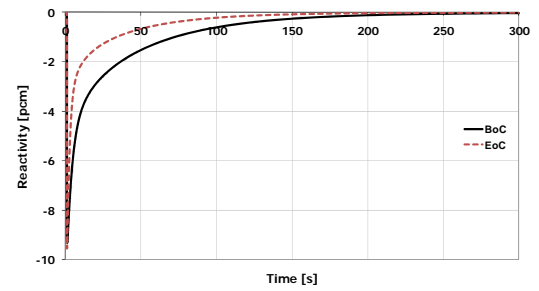
Fig. 6. Core reactivity variation following an enhancement by 10 K of core inlet temperature.

Linked, T_l radial expansion
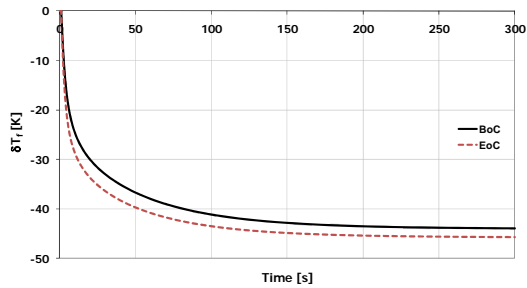
Fig. 7. Fuel average temperature variation following an enhancement by 10 K of core inlet temperature.
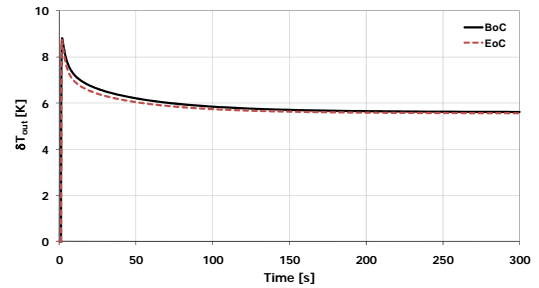
Fig. 10. Core outlet temperature variation following an enhancement by 10 K of core inlet temperature.
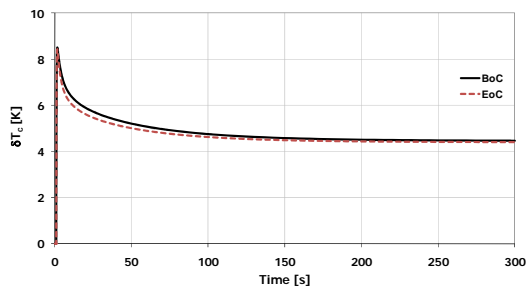
Fig. 8. Cladding average temperature variation following an enhancement by 10 K of core inlet temperature.
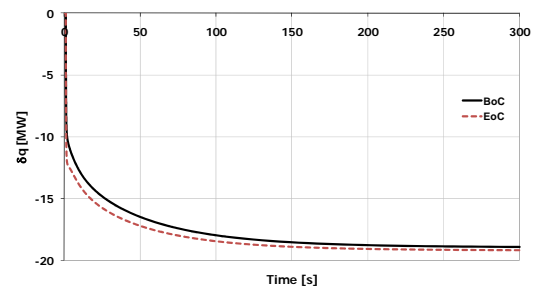
Fig. 11. Reactor power variation following an enhancement by 10 K of core inlet temperature.
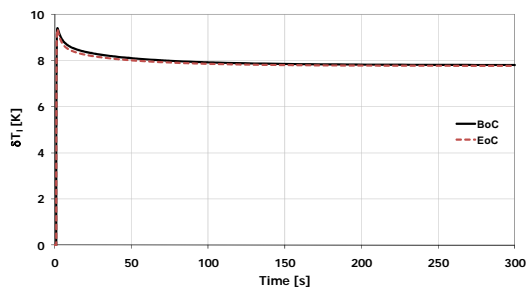
Fig. 9. Lead average temperature variation following an enhancement by 10 K of core inlet temperature.
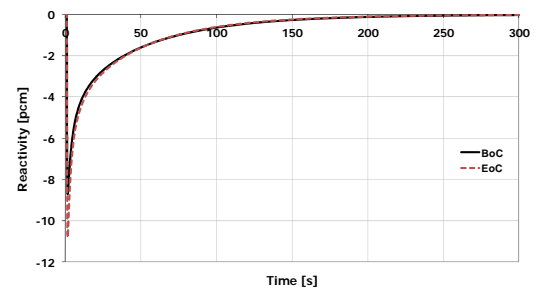
Fig. 12. Core reactivity variation following an enhancement by 10 K of core inlet temperature.

Not-linked, T_l radial expansion
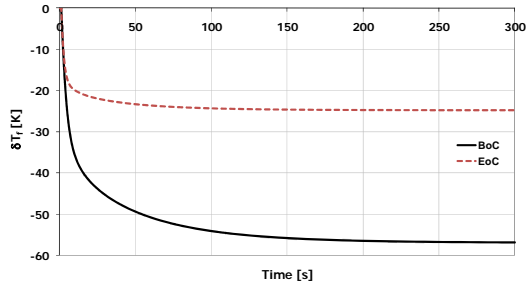
Fig. 13. Fuel average temperature variation following an enhancement by 10 K of core inlet temperature.
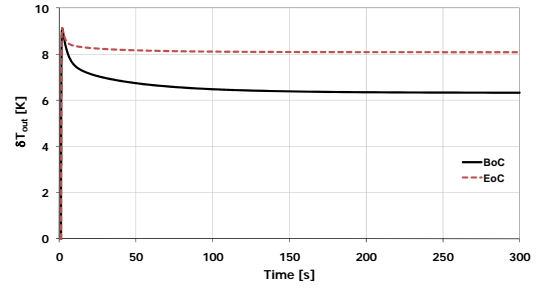
Fig. 14. Cladding average temperature variation following an enhancement by 10 K of core inlet temperature.

Fig. 15. Lead average temperature variation following an enhancement by 10 K of core inlet temperature.

Fig. 16. Core outlet temperature variation following an enhancement by 10 K of core inlet temperature.
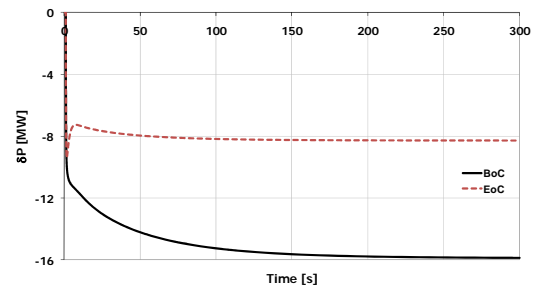
Fig. 17. Reactor power variation following an enhancement by 10 K of core inlet temperature.
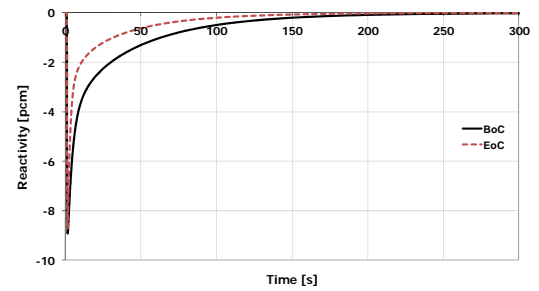
Fig. 18. Core reactivity variation following an enhancement by 10 K of core inlet temperature.

A.2. CONTROL ROD EXTRACTION

Not-linked, T$_{in}$ radial expansion
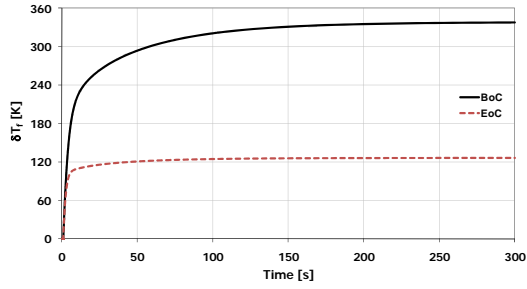
Fig. 19. Fuel average temperature variation following a step
reactivity insertion of 50 pcm.

Fig. 20. Cladding average temperature variation following a
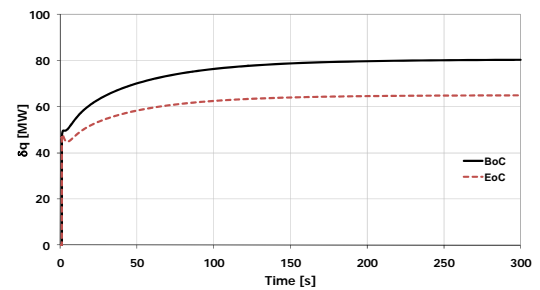step reactivity insertion of 50 pcm.

Fig. 21. Lead average temperature variation following a step
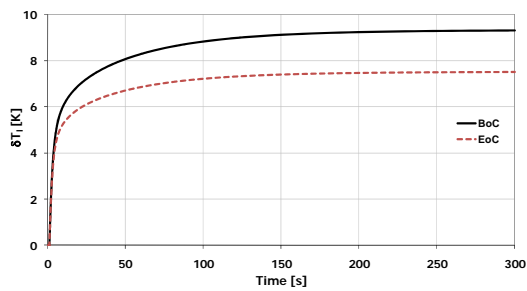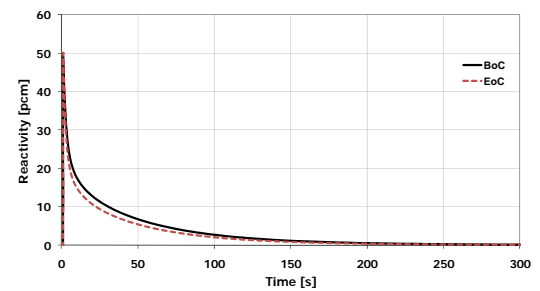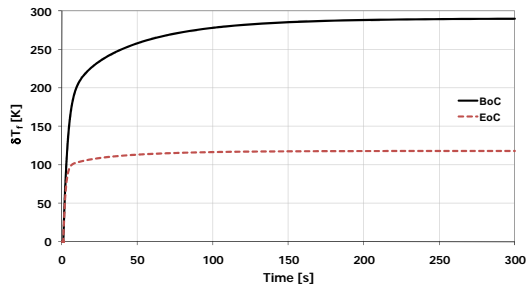reactivity insertion of 50 pcm.
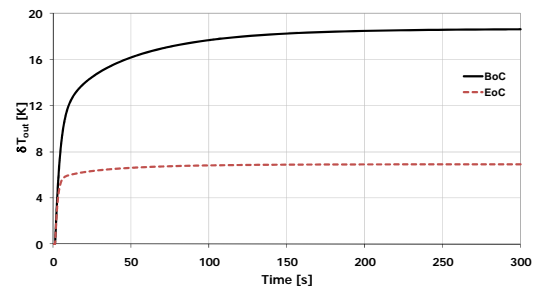
Fig. 22. Core outlet temperature variation following a step
reactivity insertion of 50 pcm.
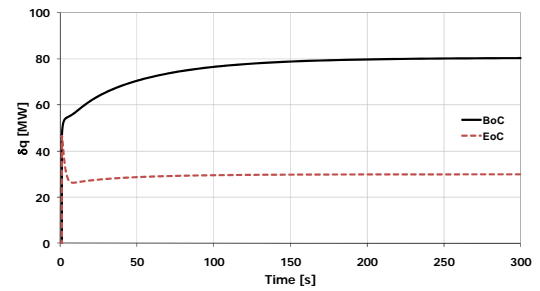
Fig. 23. Reactor power variation following a step reactivity
insertion of 50 pcm.
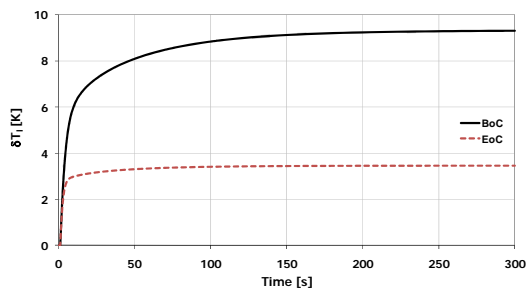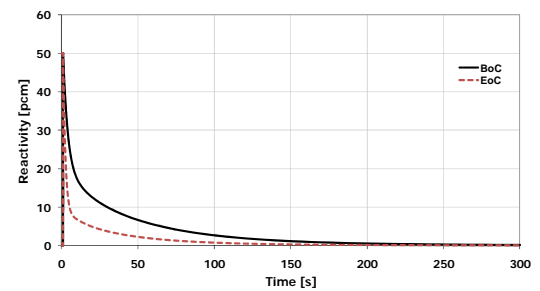
Fig. 24. Core reactivity variation following an externally
given perturbation of 50 pcm.

<u>*Linked, T_l radial expansion*</u>
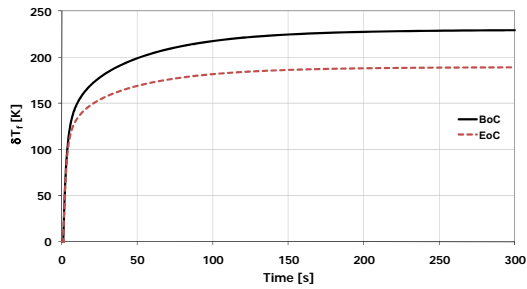
Fig. 25. Fuel average temperature variation following a step
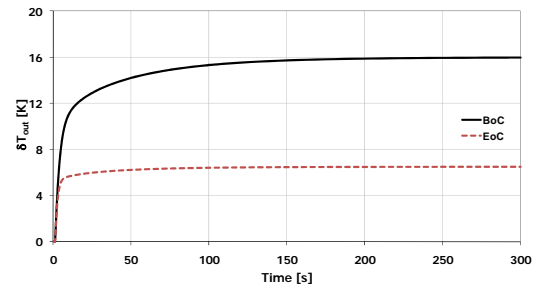reactivity insertion of 50 pcm.

Fig. 26. Cladding average temperature variation following a
step reactivity insertion of 50 pcm.

Fig. 27. Lead average temperature variation following a step
reactivity insertion of 50 pcm.
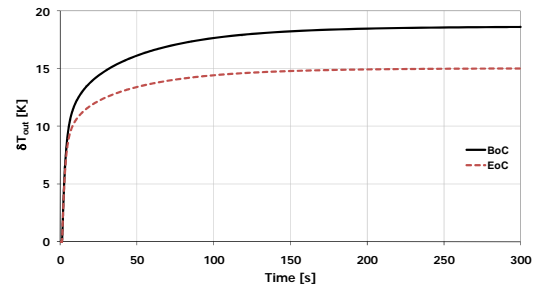
Fig. 28. Core outlet temperature variation following a step
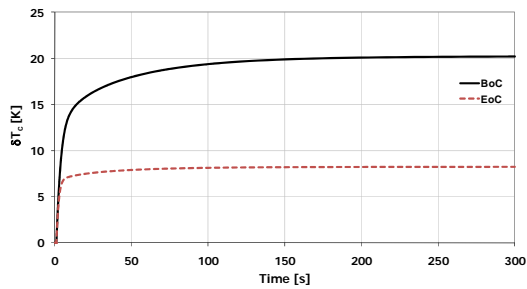reactivity insertion of 50 pcm.

Fig. 29. Reactor power variation following a step reactivity
insertion of 50 pcm.

Fig. 30. Core reactivity variation following an externally
given perturbation of 50 pcm.

Not-linked, T_l radial expansion

Fig. 31. Fuel average temperature variation following a step reactivity insertion of 50 pcm.

Fig. 32. Cladding average temperature variation following a step reactivity insertion of 50 pcm.
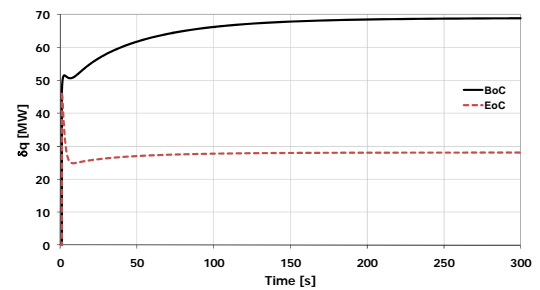

Fig. 33. Lead average temperature variation following a step reactivity insertion of 50 pcm.

Fig. 34. Core outlet temperature variation following a step reactivity insertion of 50 pcm.

Fig. 35. Reactor power variation following a step reactivity insertion of 50 pcm.
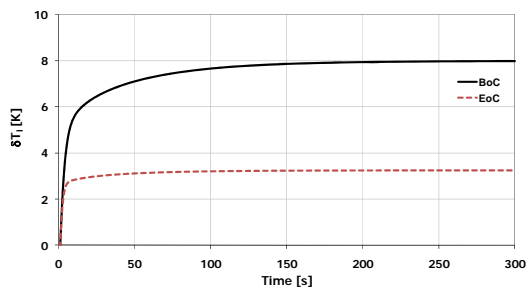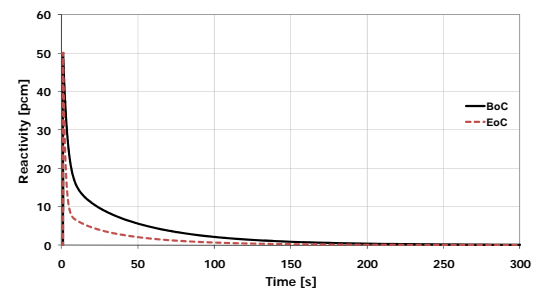

Fig. 36. Core reactivity variation following an externally given perturbation of 50 pcm.